



THE UNIVERSITY *of* EDINBURGH

Edinburgh Research Explorer

First dinosaur from the Isle of Eigg (Valtos Sandstone Formation, Middle Jurassic) Scotland

Citation for published version:

Panciroli, E, Funston, G, Holwerda, F, GeoZentrum, N, Maidment, S, Foffa, D, Larkin, N, Challands, T, Depolo, P, Goldberg, D, Humpage, M, Ross, DA, Wilkinson, M & Brusatte, S 2020, 'First dinosaur from the Isle of Eigg (Valtos Sandstone Formation, Middle Jurassic) Scotland', *Earth and environmental science transactions of the royal society of edinburgh*. <https://doi.org/10.1017/S1755691020000080>

Digital Object Identifier (DOI):

[10.1017/S1755691020000080](https://doi.org/10.1017/S1755691020000080)

Link:

[Link to publication record in Edinburgh Research Explorer](#)

Document Version:

Peer reviewed version

Published In:

Earth and environmental science transactions of the royal society of edinburgh

Publisher Rights Statement:

© The Author(s) 2020. Published by Cambridge University Press on behalf of The Royal Society of Edinburgh

General rights

Copyright for the publications made accessible via the Edinburgh Research Explorer is retained by the author(s) and / or other copyright owners and it is a condition of accessing these publications that users recognise and abide by the legal requirements associated with these rights.

Take down policy

The University of Edinburgh has made every reasonable effort to ensure that Edinburgh Research Explorer content complies with UK legislation. If you believe that the public display of this file breaches copyright please contact openaccess@ed.ac.uk providing details, and we will remove access to the work immediately and investigate your claim.



First dinosaur from the Isle of Eigg (Valtos Sandstone Formation, Middle Jurassic) Scotland

Journal:	<i>Earth and Environmental Science Transactions of the Royal Society of Edinburgh</i>
Manuscript ID	TRE-2020-0011.R1
Manuscript Type:	Spontaneous Article
Date Submitted by the Author:	n/a
Complete List of Authors:	Panciroli, Elsa; University of Oxford, Department of Earth Sciences; National Museums Scotland, Natural Sciences Department; University of Edinburgh Department of Geology and of Geophysics Funston, Gregory ; University of Edinburgh Department of Geology and of Geophysics Holwerda, Femke; Utrecht University Faculty of Geosciences; GeoZentrum Nordbayern; Royal Tyrrell Museum Maidment, Susannah; Natural History Museum Foffa, Davide; National Museums Scotland Larkin, Nigel; University of Cambridge University Museum of Zoology Challands, Thomas; University of Edinburgh, School of GeoSciences dePolo, Paige; University of Edinburgh Department of Geology and of Geophysics Goldberg, Daniel; University of Edinburgh Department of Geology and of Geophysics Humpage, Matthew; Oxford Ross, Dugald; Staffin Museum, Earth Sciences Wilkinson, Mark; University of Edinburgh Department of Geology and of Geophysics Brusatte, Stephen; University of Edinburgh, School of Geosciences; National Museums Scotland, National Museums Scotland
Keywords:	Great Estuarine Group, Bathonian, Thyreophora, histology, Sauropoda, Theropoda
Abstract:	Dinosaur body fossil material is rare in Scotland, previously known almost exclusively from Great Estuarine Group on the Isle of Skye. We report the first unequivocal dinosaur fossil from the Isle of Eigg, belonging to a Bathonian (Middle Jurassic) taxon of uncertain affinity. The limb bone NMS.Eigg.2017, is incomplete, but through a combination of anatomical comparison and osteohistology we determine it most likely represents a stegosaur fibula. The overall proportions and cross-sectional geometry are similar to the fibulae of thyreophorans. Examination of the bone microstructure reveals a high degree of remodelling and randomly distributed longitudinal canals in the remaining primary cortical bone. This contrasts with the histological signal expected of theropod or sauropod limb bones, but is consistent with previous studies of thyreophorans, specifically stegosaurs. Previous dinosaur material from Skye and broadly contemporaneous sites in England belongs to this group, including <i>Loricatosaurus</i> and <i>Sarcolestes</i> and a number of indeterminate stegosaur specimens. Theropods such as <i>Megalosaurus</i> and sauropods such as <i>Cetiosaurus</i> are also known from these localities. Although we find strong evidence for a stegosaur affinity, diagnostic features are not observed on NMS.Eigg.2017, preventing us from referring it to any known genera. The presence of this large-bodied

	stegosaur on Eigg adds a significant new datapoint for dinosaur distribution in the Middle Jurassic of Scotland.

SCHOLARONE™
Manuscripts

1 First dinosaur from the Isle of Eigg (Valtos Sandstone Formation, Middle Jurassic)
2 Scotland

3

4 Elsa Panciroli^{1,2,3*}, Gregory F. Funston³, Femke Holwerda^{4,5,6}, Susannah C. R.
5 Maidment⁷, Davide Foffa², Nigel Larkin⁸, Tom Challands³, Paige E. dePolo³, Daniel
6 Goldberg³, Matthew Humpage⁹, Dugald Ross¹⁰, Mark Wilkinson³ Stephen L.
7 Brusatte^{2,3}

8

9 1 Department of Natural Sciences, University of Oxford, South Parks Road, Oxford,
10 OX1 3AN

11 2 Natural Sciences Department, National Museum of Scotland, Edinburgh, Scotland,
12 UK, EH1 1JF

13 3 School of Geosciences, University of Edinburgh, Scotland, UK, EH9 3FE

14 4 Department of Geosciences, Utrecht University, Princetonlaan 8a, 3584 CB
15 Utrecht, The Netherlands

16 5 Fachgruppe Paläoumwelt, GeoZentrum Nordbayern, Friedrich-Alexander-
17 Universität Erlangen-Nürnberg, Loewenichstr. 28, 91054 Erlangen, Germany

18 6 Royal Tyrrell Museum of Palaeontology, Drumheller, Alberta T0J 0Y0, Canada

19 7 Department of Earth Sciences, Natural History Museum, Cromwell Road, London,
20 SW7 5BD, United Kingdom

21 8 Cambridge University Museum of Zoology, Downing Street, Cambridge CB2 3EJ,
22 UK

23 9 Oxford, England, UK

24 10 Staffin Museum, Ellishadder, Staffin, Isle of Skye IV51 9JE, UK

25

26 *Corresponding author: elsa.panciroli@earth.ox.ac.uk

27

28 RH: First dinosaur from the Isle of Eigg, Scotland

29

30

31 ABSTRACT: Dinosaur body fossil material is rare in Scotland, previously known
32 almost exclusively from Great Estuarine Group on the Isle of Skye. We report the
33 first unequivocal dinosaur fossil from the Isle of Eigg, belonging to a Bathonian
34 (Middle Jurassic) taxon of uncertain affinity. The limb bone NMS.Eigg.2017, is
35 incomplete, but through a combination of anatomical comparison and osteohistology
36 we determine it most likely represents a stegosaur fibula. The overall proportions
37 and cross-sectional geometry are similar to the fibulae of thyreophorans.
38 Examination of the bone microstructure reveals a high degree of remodelling and
39 randomly distributed longitudinal canals in the remaining primary cortical bone. This
40 contrasts with the histological signal expected of theropod or sauropod limb bones,
41 but is consistent with previous studies of thyreophorans, specifically stegosaurs.
42 Previous dinosaur material from Skye and broadly contemporaneous sites in
43 England belongs to this group, including *Loricatosaurus* and *Sarcolestes* and a
44 number of indeterminate stegosaur specimens. Theropods such as *Megalosaurus*
45 and sauropods such as *Cetiosaurus* are also known from these localities. Although
46 we find strong evidence for a stegosaur affinity, diagnostic features are not observed
47 on NMS.Eigg.2017, preventing us from referring it to any known genera. The
48 presence of this large-bodied stegosaur on Eigg adds a significant new datapoint for
49 dinosaur distribution in the Middle Jurassic of Scotland.

50

51 Key Words: Great Estuarine Group, Bathonian, Thyreophora, histology, Sauropoda,
52 Theropoda,

53

54

55 Dinosaurs first evolved in the Late Triassic, but remained a relatively sparse
56 component of ecosystems until after the end-Triassic mass extinction. During the
57 Middle Jurassic, the group underwent a significant evolutionary radiation and they
58 became the dominant vertebrates on land for the subsequent 100 million years
59 (Benson *et al.* 2014; Benson 2018). However, our understanding of the mode,
60 tempo, and evolutionary drivers of this radiation are hindered by the globally sparse
61 fossil record for dinosaurs at this time. For example, the Paleobiology Database
62 (www.paleobiodb.org) records just 430 occurrences of Middle Jurassic dinosaurian
63 body fossils globally. In contrast, the much better-known Late Jurassic record
64 preserves 2,100 occurrences of Dinosauria (data downloaded June 2020). This
65 makes all contributions to the Middle Jurassic dinosaur fossil record significant.

66 The Inner Hebrides of Scotland yield rare Middle Jurassic dinosaur remains,
67 but until now these have been exclusively from the Isle of Skye. The Bajocian–
68 Bathonian Great Estuarine Group on Skye provides a vivid picture of the diverse
69 Middle Jurassic ecosystem of the Inner Hebrides. It comprises a series of lagoonal
70 and deltaic sedimentary rocks (Andrews 1985) that have yielded a wealth of
71 vertebrate material, including marine, terrestrial and flying archosaurs, turtles,
72 squamates, lissamphibians, tritylodontids and mammaliaforms (e.g. Evans *et al.*
73 2006; Anquetin *et al.* 2009, 2010; Wills *et al.* 2014; Young *et al.* 2016a; Yi *et al.*
74 2017; Panciroli 2017a, b, 2018a, b, 2019).

75 Dinosaur body fossils in the Great Estuarine Group remain exceptionally rare
76 and are often fragmentary (see review in Clark [2018]). From the Bathonian Valtos
77 Sandstone Formation they include a sauropod limb bone (Clark *et al.* 1995; Liston
78 2004), a sauropod tooth (Clark & Gavin 2016), two theropod teeth (Brusatte & Clark
79 2015; Young *et al.* 2019), and a possible basal coelurosaurian theropod caudal
80 vertebra (Brusatte & Clark 2015). Finds from other formations within the Great
81 Estuarine Group and underlying units include a theropod limb bone (Benton *et al.*
82 1995), an isolated theropod tooth (Young *et al.* 2019), isolated sauropod teeth
83 (Barrett *et al.* 2006), and a thyreophoran proximal ulna and radius (Clark 2001).
84 Dinosaur ichnofossil tracks range from isolated tracks on loose boulders (Andrews &
85 Hudson 1984; Clark *et al.* 2005; Clark & Gavin 2016), to extensive *in situ* trackway
86 sites, including from the Valtos Sandstone Formation (Clark *et al.* 2004; Marshall
87 2005; Brusatte *et al.* 2015; dePolo *et al.* 2018, 2020).

88 The Isle of Eigg has long been recognised for its fossils, particularly the ‘Hugh
89 Miller Reptile Bed’ named for the prolific Victorian stonemason turned
90 palaeontologist, geologist and writer, Hugh Miller (1802-1856) who discovered it
91 (Miller 1858). The reptile bed is part of the Bathonian Lealt Shale Formation
92 (formerly ‘Estheria Shales’, Hudson 1962, 1963), which underlies the Valtos
93 Sandstone Formation (Andrews 1985; Barron *et al.* 2012). Vertebrate fossils from
94 the Lealt Shale Formation mainly comprise isolated skeletal and dental remains of
95 sharks, marine turtles, crocodylomorphs, and plesiosaurs (Hudson 1966; Benton
96 1995). A single purported dinosaur tooth from Eigg was mentioned by Rees and
97 Underwood (2005), but this specimen was not figured and has subsequently been
98 lost, so the identification cannot be confirmed. Despite extensive explorations of the

99 island by Miller and contemporaries, and subsequent attention from geologists and
100 palaeontologists in the latter half of the 20th century (e.g. Hudson 1962, 1963, 1966;
101 Harris & Hudson 1980; Andrews 1985), no archosaur material has been discovered
102 in any of the other exposed sections of the Great Estuarine Group on Eigg until now.

103 Herein we describe the first unequivocal Mesozoic dinosaur specimen to be
104 found in Scotland outside of Skye. The specimen is an indeterminate limb bone—
105 probably from a stegosaur—that was found in shoreline exposures of the Valtos
106 Sandstone Formation on the Isle of Eigg. The specimen described here is poorly
107 preserved, hindering higher level taxonomic assignment, but this limitation does not
108 negate the significance of this fossil both in the context of the Scottish dinosaur body
109 fossil record, and for our knowledge of Middle Jurassic dinosaur palaeo-distribution.

110

111 1. Geological Setting

112

113 The Great Estuarine Group (Harris & Hudson 1980; ‘Great Estuarine Series’ of Judd
114 [1878, p.722]) crops out in the Scottish Inner Hebridean islands of Skye, Muck, Eigg
115 and Raasay (though contemporaneity of formations between the isles is by no
116 means certain) (Fig. 1). It comprises six formations (the Cullaidh Shale Formation,
117 Elgol Sandstone Formation, Lealt Shale Formation, Valtos Sandstone Formation,
118 Duntulm Formation and the Kilmaluag Formation) of Bajocian–Bathonian (Middle
119 Jurassic) age, consisting of sedimentary rocks dominated by sandstone and
120 mudstone, with subordinate shelly, algal and dolomitic limestone beds (Harris &
121 Hudson 1980; Barron *et al.* 2012). Environments represented include shallow
122 marine, saline, and freshwater lagoons, with tidally influenced littoral lagoons, fluvial
123 delta lobes, and alluvial floodplains and mudflats (Barron *et al.* 2012).

124 The Valtos Sandstone Formation is named after the village of Valtos on the
125 Trotternish Peninsula on the Isle of Skye, near the type section [NG 517 638 to NG
126 509 653] (Harris & Hudson 1980: 240–243). It is underlain by the Lealt Shale
127 Formation and overlain by the Duntulm Formation. Fossils found include:
128 invertebrates such as the bivalve *Neomiodon* and gastropod *Viviparus*; trace fossils
129 *Lockeia*, *Monocraterion*, *Planolites*, *Thalassinoides* and tridactyl and ovoid footprints;
130 coniferous wood; and fragmentary dinosaur and crocodyliform body fossils (Hudson
131 & Harris 1979; Andrews & Hudson 1985; Clark *et al.* 1995; Barron *et al.* 2012;
132 Brusatte & Clark 2015; Clark & Gavin 2016; Young *et al.* 2016a). The Valtos
133 Formation represents a tidally influenced shallow littoral lagoon, frequently inundated
134 by fluvial delta lobes, and with evidence of periodic emergence (Barron *et al.* 2012).
135 This interpretation is supported by brackish to freshwater palynomorphs such as
136 *Botryococcus* (Riding *et al.* 1991).

137 A section of the Valtos Sandstone Formation is exposed on the northwestern
138 shore of the Isle of Eigg at Camas Sgiotaig (the ‘singing sands’) and the bay of Laig
139 [NM 468 905 to NM 472 885]. The limb-bone NMS.Eigg.2017 was found in a loose
140 block within Camas Sgiotaig, in a broken, but originally sub-spherical, calcite-
141 cemented sandstone concretion (*sensu* Wilkinson 1992). On the Isle of Eigg, such

142 concretions are only known from the Valtos Sandstone Formation, confirming the
143 provenance of the specimen.

144

145

146 **2. Materials and Methods**

147

148 The limb-bone NMS.Eigg.2017 is part of the collection at National Museums
149 Scotland (NMS), Edinburgh, UK. It was found by EP on a loose boulder below the
150 high tide line south of Camas Sgiotaig on the Isle of Eigg in May 2017, during
151 fieldwork funded by the National Geographic Society, including team members SLB,
152 EP, TJC, PEdP, DF, and MW. It was subsequently collected under permit by SLB,
153 DR, and DG, using a rock saw to extract the specimen. Preparation was carried out
154 by NL: the bone was consolidated using Paraloid B72 at 5-10% in acetone, then
155 pneumatic circular saws followed by pneumatic pens were used to remove
156 surrounding matrix. A small <1 cm section of the bone was accidentally removed
157 during removal of excess matrix (Fig. 2C). The natural mould of the missing mid-
158 section of the bone was filled in with Jesmonite acrylic resin with some fibreglass
159 matting with grey pigment.

160 A photogrammetric model of NMS.Eigg.2017 was created by MH using
161 photographs taken on a Nikon D5300 and uploaded and reconstructed in Agisoft
162 Photoscan Professional Version 1.4.5. The resulting mesh was repaired and
163 optimised in Blender 2.8.1 and then exported in .fpx format. This can be accessed
164 freely on Sketchfab at [LINK].

165 A portion of the midshaft was removed at a natural break for osteohistological
166 analysis by GFF, and a transverse thin section made following a modified
167 petrographic sectioning procedure (Lamm 2013). The piece was embedded in
168 Buehler Epothin II epoxy resin under a vacuum (-1 bar) and left to cure at room
169 temperature for 24 hours. The block was sectioned in a transverse plane using a
170 Buehler Isomet 1000 Precision Saw with a table saw attachment and a diamond-
171 tipped wafering blade. The cut billet was mounted to a polycarbonate plastic slide
172 using Buehler Epothin II epoxy, which was left to cure at room temperature for 12
173 hours. The mounted billet was resectioned to a thickness of 0.7 mm using a Buehler
174 Isomet 1000 Precision Saw. The re-sectioned slide was hand-ground on a glass
175 plate using a sequence of 220-grit, 600-grit, and 1200-grit Silicon Carbide abrasive
176 powders, until the desired optical contrast was achieved. The final slide thickness is
177 ~180 µm. The slide was polished on a short nap cloth and on a nap cloth with
178 mineral oil to improve optical clarity.

179 The slide was photographed using a Nikon D7200 DSLR camera with a
180 Nikkor 60 mm Micro lens and a Nikon SB-600 Speedlight to produce transmitted
181 light. Detailed images were taken using a Leica DMLP Transmitted Light Polarizing
182 Microscope under normal light using Leica Application Suite 4. The polycarbonate
183 sheet used for the slide is anisotropic, which interferes with cross-polarization of the
184 thin-section, so only images under normal light were taken. Images were stitched
185 together using Adobe Photoshop 2020. Where adjustments to contrast, brightness,

186 or colour balance **were required**, these modifications were applied to the entire
 187 image. Osteocyte lacunar density was calculated using the method of Cullen *et al.*
 188 (2014). Histological terminology follows Francillon-Vieillot *et al.* (1990) and Padian
 189 and Lamm (2013).

190 Measurements of NMS.Eigg.2017 were checked using photogrammetry
 191 models. Measurements **and some figures** for **the comparative** taxa **were** taken from
 192 Benson (2010), Holwerda *et al.* (in press) **and** Remes *et al.* (2009) **in combination**
 193 **with the authors' (EP, FH, SCRM)** own photographs of specimens.

194
 195 **Institutional Abbreviations.** CGP, Council for Geosciences, Pretoria, South
 196 Africa; ISIR, Indian Statistical Institute, Kolkata, India; MACN, Museo Argentino de
 197 Ciencias Naturales, Buenos Aires, Argentina; MOR, Museum of the Rockies,
 198 Montana, USA; NHMUK (**previously BMNH**), Natural History Museum, London, UK;
 199 NMS National Museums Scotland, Edinburgh, UK; OUMNH, Oxford University
 200 Museum of Natural History, Oxford, UK; PVL, Paleontologia de Vertebrados Lillo,
 201 Universidad Nacional de Tucuman, Tucuman, Argentina; QMF, Queensland Museum,
 202 Brisbane, Australia.

203 204 **3. Systematic Palaeontology**

205 206 SYSTEMATIC PALAEOLOGY

207 DINOSAURIA OWEN, 1842

208 Ornithischia Seeley, 1887

209 Thyreophora Nopcsa, 1915 (sensu Norman, 1984)

210
 211 **Material.** NMS.Eigg.2017, an isolated hind limb bone (Fig. 2).

212 **Locality.** Bathonian (Middle Jurassic) Valtos Sandstone Formation, Great
 213 Estuarine Group. Found on **a** loose boulder on **the** shoreline south of Camas
 214 Sgiotaig, Isle of Eigg, Scotland.

215 **Description.** NMS.Eigg.2017 is badly eroded along most of its length where
 216 exposed to weathering by the sea. It is also missing the proximal and distal ends,
 217 and is slightly compressed along its length. The total preserved length is 64 cm, and
 218 the bone is broken into two halves. Without a definitive identification, it is not
 219 possible to say which is the proximal or distal end. One half of the bone has been
 220 worn longitudinally, leaving a depth of ~5 cm of bone and exposing the internal
 221 structure (Fig. 2). The centre of the shaft is missing, but there was a natural mould of
 222 the shaft in the rock, which was used to make a reconstruction (Fig. 2) The moulded
 223 section is approximately 14 cm in length and 7.3 cm at the narrowest **transverse**
 224 **width**. There is a **longitudinal** ridge on the bone shaft, beginning near the break and
 225 extending to **the margin of** one of the broken ends (Fig. 2C), **where** the bone flares
 226 laterally on one side. **The** extent of this lateral projection is unclear **because** the rest
 227 of the bone is broken and missing. At least two potential tooth marks are visible on
 228 the opposite end of the bone, measuring ~2 cm in length and ~0.2 cm deep (Fig.

229 3A). A layer of small molluscs (probably *Neomiodon*) are present on the underside of
230 the bone (Fig. 3B).

231 In the absence of the epiphyses and without a **complete** shaft of the bone,
232 identification presents a challenge. Based on dimensions, comparative anatomy and
233 histology (see below) we suggest that NMS.Eigg.2017 is probably a stegosaur fibula.

234

235

236 4. Possible Identity of NMS.Eigg.2017

237

238 4.1 Marine Reptiles and Crocodylomorphs

239 A variety of marine reptile (ichthyosaurs and plesiosaurs) and various
240 crocodylomorph fossils are known from the Middle Jurassic formations of the Inner
241 Hebrides, mostly from the Isle of Skye (Lee & Buckman 1920; Arkell 1933; Hudson
242 1966; Martill 1985; Clark *et al.* 1993; Benton *et al.* 1995; Brusatte *et al.* 2015; Yi *et al.*
243 2017; Young *et al.* 2016a). Marine reptile remains from the Isle of Eigg comprise
244 disarticulated plesiosaurian bones from the 'Hugh Miller Bonebed' (Miller 1858;
245 Hudson 1966).

246 Despite the presence of marine reptiles and crocodylomorphs in these
247 outcrops, we do not consider NMS.Eigg.2017 to belong to any of these groups. The
248 large size of NMS.Eigg.2017 excludes it from belonging to any of the small-bodied
249 crocodylomorph taxa found in the Middle Jurassic of the Hebrides (e.g. Young *et al.*
250 2016a; Yi *et al.* 2017). Although larger-bodied thalattosuchian crocodylomorphs
251 (teleosauroids and metriorhynchoids) have been recovered from contemporaneous
252 Middle Jurassic formations elsewhere (Mannion *et al.* 2015; Wilberg 2015; Johnson
253 *et al.* 2019), no thalattosuchians have yet been reported from Scotland. Even the
254 **largest thalattosuchian femora are much** smaller than NMS.Eigg.2017 (e.g. ~45 cm
255 in *Lemmysuchus obtusidens* and *Machimosaurus mosae*; Hua 1999, Johnson *et al.*
256 2017; Young *et al.* 2016b). **The fibula/tibia is shortened compared to their femur—a**
257 **modification linked to their aquatic lifestyle (Foffa *et al.* 2019). In addition,**
258 **NMS.Eigg.2017 has several features that make it unlikely to belong to this clade. For**
259 **example** thalattosuchian femora have a sigmoidal profile with an **oval** cross-section,
260 which is not seen in NMS.Eigg.2017 (Andrews 1913; Hua & De Buffrenil 1996),
261 **although compression and poor preservation make the cross sectional geometry**
262 **difficult to assess.** In large thalattosuchians the cranial bones attained a **length**
263 comparable to NMS.Eigg.2017, **but** the absence of articular facets, alveoli, or dermal
264 ornamentation that characterise most thalattosuchian cranial bones (Andrews 1913)
265 make this identification incompatible with the morphology seen here. **NMS.Eigg.2017**
266 **differs histologically from crocodylomorphs in the predominance of fibrolamellar bone**
267 **with abundant osteons and the absence of parallel-fibered bone in the cortex.**
268 **Whereas fibrolamellar or woven bone is occasionally present in some**
269 **crocodylomorphs (Woodward *et al.* 2014; Cubo *et al.* 2017), their cortices are usually**
270 **formed exclusively of parallel-fibered or lamellar bone with simple vascular canals or**
271 **sparse primary osteons (Hua and De Buffrenil 1996; Andrade and Sayão 2014;**
272 **Sayão *et al.* 2016; Cubo *et al.* 2017).**

273 For these reasons we preclude this bone from being identified as that of a
274 crocodylomorph.

275 The large size of NMS.Eigg.2017 also rules out attribution to an ichthyosaur
276 or plesiosaur. **Furthermore the overall shape of NMS.Eigg.2017 does not match that**
277 **of marine reptiles.** The limbs of **the latter** are highly modified for underwater
278 propulsion, **being** reduced or absent compared to terrestrial animals—as in all fully
279 marine tetrapods (Andrews 1910). Plesiosaur and ichthyosaur limbs have short,
280 robust humeri and femora with flared proximal and/or distal ends. The propodeal
281 bones (radius, ulna, tibia, fibula) of these taxa are highly modified into short, often
282 polygonal elements in the paddle (McGowan & Motani 2003; Benson 2013). The
283 microstructure of marine reptile bones is also significantly different from that of
284 terrestrial animals, **typically showing either osteoporotic or pachyostotic textures**
285 (Hua & De Buffrenil 1996; Houssaye 2013) and does not match that found in the
286 histological section of NMS.Eigg.2017 (see 5.0 Histology).

287

288 4.2 Theropoda

289 Theropod dinosaurs were the primary terrestrial carnivores during the Middle
290 Jurassic. **They ranged** from those with small body masses similar to many extant
291 birds, to medium to large sized genera like *Megalosaurus bucklandii* (Benson 2010),
292 which reached body masses of ~1.4 tons (Benson *et al.* 2014) and lengths of ~8-9
293 meters, and *Eustreptospondylus oxoniensis* (Sadlier *et al.* 2008). **Both of these taxa**
294 **are well-known basal tetanurans from the Middle Jurassic of England.** Medium to
295 large ceratosaurians and potentially mid-sized basal coelurosaurs (tyrannosauroids)
296 were also present **globally** during this time (see review by Hendrickx *et al.* 2015).

297 If NMS.Eigg.2017 is a theropod dinosaur, it would belong to a mid-to-large-
298 sized taxon. Based on size and proportions, the only theropod skeletal element
299 NMS.Eigg.2017 could be is a femur. The length to width ratio is similar to the femur
300 of Middle Jurassic *Megalosaurus bucklandii* (Benson 2010: fig 16) and
301 *Eustreptospondylus oxoniensis* (Sadlier *et al.* 2008: fig. 19) (Table 1, Fig. 4A-D). The
302 lateral projection at one end of NMS.Eigg.2017 may correspond to the neck of the
303 femoral head (with the head missing), and the opposite end may represent the distal
304 end of a femur with the beginning of an epicondylar (flexor or extensor) groove (Fig.
305 4). However, the bone lacks the prominent lesser (=anterior) and fourth trochanters
306 that characterize theropod femora. The longitudinal ridge on one half of
307 NMS.Eigg.2017 may be the base of a lesser trochanter, but the lesser trochanters of
308 mid-to-large-sized theropods project strongly from the anterior surface of the bone,
309 whereas this ridge is less prominent in NMS.Eigg.2017. **Even the less pronounced**
310 **lesser trochanter of *Eustreptospondylus* (Fig. 3C-D) is more pronounced than in**
311 **NMS.Eigg.2017. We consider it** unlikely that the ridge is a damaged remnant of a
312 more pronounced trochanter, as its surface is smooth and unbroken. It is also
313 unlikely that a more prominent lesser trochanter was present in life but not
314 observable because the bone has broken distal to it. If NMS.Eigg.2017 is a theropod
315 femur, the lateral projection of the presumed proximal end indicates that only a
316 moderate portion of the head is missing proximally. Therefore, the region that would

317 have included the trochanter is preserved, but lacks this predominant feature. The
318 fourth trochanter should also be visible along the posterior surface of the shaft, but
319 appears to be absent. Although there is a large portion of the mid-shaft missing—
320 meaning we cannot completely rule out the presence of a fourth trochanter—overall
321 we consider the identification of NMS.Eigg.2017 as a theropod femur unlikely.

322 NMS.Eigg.2017 is much larger, longer and more slender than the humerus,
323 radius or ulna of *Megalosaurus bucklandii* (Benson 2010: figs 12-13) (Fig. 4E),
324 *Eustreptospondylus* (Sadlier *et al.* 2008: fig 16), and other mid- to large-bodied
325 theropods, which were all bipedal animals with much shorter forelimbs than hind
326 limbs. Although NMS.Eigg.2017 has a similar length and width as the tibia of
327 *Megalosaurus*, NHMUK PV OR31809 (Fig. 4F-G), it lacks the twist of the shaft from
328 proximal to distal ends observed in the tibia of *Megalosaurus*, *Eustreptospondylus*
329 (Sadlier *et al.* 2008: fig. 20), or other theropods, and also lacks any sign of the
330 prominent cnemial and fibular crests. NMS.Eigg.2017 also does not match the
331 gracile and distally tapering morphology of theropod fibulae.

332 Histological analysis does not support the identification of NMS.Eigg.2017 as
333 belonging to a theropod. The cancellous medullary cavity of NMS.Eigg.2017 is unlike
334 the limb bones of most theropod dinosaurs, which are hollow. The pectoral and
335 pelvic girdle elements of theropods have a cancellous medullary cavity, but it is
336 difficult to reconcile the gross morphology of NMS.Eigg.2017 with these bones:
337 theropod scapulae are flat, straplike bones, which is not the case in NMS.Eigg.2017,
338 and there is no evidence of a pubic apron, pubic boot, or obturator process in
339 NMS.Eigg.2017, which eliminates a pubis or ischium as a candidate.

340

341

342 4.3 Sauropoda

343 The body fossil record for Middle Jurassic Sauropoda is relatively scarce compared
344 to that of the Late Jurassic or Cretaceous. Material is known from China, India, North
345 Africa, Argentina, and the UK. From the Bajocian–Bathonian of Oxfordshire and
346 Gloucestershire sauropods are represented by *Cetiosaurus oxoniensis* (Upchurch
347 and Martin 2002, 2003). Finds from the northwest of Scotland provide additional
348 indeterminate sauropod material, comprising incomplete limb elements and single
349 teeth (Clark *et al.* 1995; Liston 2004; Barrett *et al.* 2006; Clark and Gavin, 2016;
350 Clark, 2018).

351 The small size of NMS.Eigg.2017 makes it likely that if it is a sauropod limb
352 bone, it represents a juvenile animal. The femora of contemporaneous sauropods
353 such as *Cetiosaurus* and *Patagosaurus fariasi* are more robust than NMS.Eigg.2017,
354 with a lower length to width ratio (Fig. 5A, Table 1). Cetiosaurid femora, even in
355 juveniles, are usually anteroposteriorly flattened and mediolaterally wide, creating an
356 elliptical cross-section (Holwerda *et al.* in press). This shape contrasts with
357 NMS.Eigg.2017, which has a more gracile and rounded midshaft (Fig. 2). However,
358 features congruent with a sauropod femur include the curved, lateral projection at
359 one end of NMS.Eigg.2017, which may correspond to the base of the greater
360 trochanter, and the groove visible at the opposite end, which may represent the

361 epicondylar groove at the distal end of the femur (Fig. 2B-C). The femur of Early
362 Jurassic sauropod taxon *Barapasaurus tagorei* has closer proportions to
363 NMS.Eigg.2017 (Table 1, Fig. 5B-C), suggesting that if NMS.Eigg.2017 is a
364 sauropod femur it belonged to a gracile taxon, and possibly not a cetiosaurid—
365 *Barapasaurus* is currently placed outside of the cetiosaurid clade (Holwerda & Pol
366 2018).

367 If NMS.Eigg.2017 belongs to a sauropod, we consider it most likely to be a
368 fibula, as they are similar in length to width ratio to NMS.Eigg.2017 (Table 1).
369 Sauropod fibulae bear a posterior projection on the distal end of the bone above the
370 astragalar articular surface, as seen most clearly in *Spinophorosaurus nigeriensis*
371 (Remes *et al.* 2009) (Fig. 5G), but also to a lesser extent in *Cetiosaurus oxoniensis*
372 (Fig. 5D). This feature may correspond to the lateral projection at one end of
373 NMS.Eigg.2017 (Fig. 3). Moreover, NMS.Eigg.2017 possesses a ridge which may
374 correspond to the ridge for the accommodation of the tibia, similar to those in fibulae
375 of the contemporaneous *Cetiosaurus* (Fig. 5D), and of the possibly Oxfordian
376 *Rhoetosaurus brownei* (Fig. 5E, F). If that interpretation is correct, it would mean this
377 end of NMS.Eigg.2017 corresponds to the proximal half. The somewhat triangular
378 shape of this 'proximal' end of NMS.Eigg.2017 is similar to that in the juvenile
379 *Cetiosaurus* OUMNH J.29807 and *Rhoetosaurus* QMF 1659.

380 The extreme midshaft compression and proximal and distal flaring of the
381 humerus in sauropods is not present in NMS.Eigg.2017. All sauropods show this
382 morphology, even among juvenile individuals such as *Tazoudasaurus naimi* Pt-1
383 (Allain & Aquesbi 2008) (Fig. 5H, I). Therefore, identification of NMS.Eigg.2017 as a
384 sauropod humerus can be ruled out. There is no proximal flaring of the bone, as
385 seen in the cnemial crest of sauropod tibiae. NMS.Eigg.2017 does not possess the
386 slight sinusoidal curvature or proximal mediolateral widening and distal posterolateral
387 widening seen in the radius of *Cetiosaurus oxoniensis* OUMNH J.13611 (Fig. 5K).
388 Sauropod radii are oval in cross-section proximally (Upchurch 2004), whereas
389 NMS.Eigg.2017 is more triangular.

390 Although the length to width ratio is similar between NMS.Eigg.2017 and
391 sauropod ulnae (Table 1), and there is a similar triangular cross section near the
392 proximal end of the bone, NMS.Eigg.2017 lacks the narrow distal end, as well as the
393 triradiate anteromedial and anterolateral proximal expansions seen in sauropod
394 ulnae, e.g. *Cetiosaurus oxoniensis* OUMNH J.13611 (Fig. 5J).

395

396

397 4.4 Ornithischia

398 The Middle Jurassic body fossil record of Ornithischia is restricted to small, bipedal
399 forms (e.g. Ruiz-Omenaca *et al.* 2006), with the exception of the armoured
400 dinosaurs, Thyreophora, which were the first ornithischians to attain large body mass
401 and quadrupedality (Galton & Upchurch 2004; Barrett & Maidment 2017).

402 Thyreophoran remains are known from Middle Jurassic deposits in the UK, such as
403 *Loricatosaurus priscus* and *Sarcolestes leedsi* from the Callovian Oxford Clay
404 Formation (Galton 1983, 1985; Maidment *et al.* 2008), indeterminate stegosaur

405 remains from the Sharp's Hill Formation of Oxfordshire (Boneham & Forsey 1992),
406 and body fossils of thyreophorans from the Great Estuarine Group of the Isle of Skye
407 (Clark 2001). There are also trackways attributed to the ichnogenus *Deltapodus* from
408 Skye (dePolo *et al.* 2020) and the Middle Jurassic of Yorkshire (Whyte *et al.* 2007),
409 attributed to a stegosaur trackmaker. Possible larger-bodied ornithopod footprints
410 have recently been suggested for some of the trackways on Skye (dePolo *et al.*
411 2020), but no conclusive evidence for their presence is currently known.

412 The femora of thyreophorans are **proportionally short and robust** with rounded
413 shaft cross-sections (Fig. 6A, B). In contrast, the shaft of NMS.Eigg.2017 is slender
414 and elongate, and flattened on one side (although this may have been accentuated
415 by crushing). Humeri in thyreophorans are characterised by prominent deltopectoral
416 crests that occupy much of the length of the bone, and flared distal ends (Fig. 6C,
417 D), unlike the shape in NMS.Eigg.2017. The ulnae of thyreophorans are short,
418 **proportionally short and robust** and proximally triradiate (Fig. 6E, F), unlike
419 NMS.Eigg.2017, and the radii are shorter and much less slender than
420 NMS.Eigg.2017 (Fig. 6G, H). The cross-sectional geometry of NMS.Eigg.2017 is
421 similar to the tibiae of thyreophorans (Fig. 6I, J) although the proximal and distal
422 ends are much more flared than in NMS.Eigg.2017.

423 NMS.Eigg.2017 is similar in overall proportions and cross-sectional geometry
424 to the fibulae of thyreophorans (Fig. 6I, K). It is possible, therefore, that
425 NMS.Eigg.2017 is a fibula of a thyreophoran dinosaur. However, there are no
426 thyreophoran synapomorphies of the fibula present (Raven & Maidment 2017) and
427 so NMS.Eigg.2017 cannot be unequivocally referred to Thyreophora by comparative
428 anatomy alone (but see 5. Osteohistology).

429

430 5. Osteohistology

431

432 A transverse thin section of NMS.Eigg.2017 shows it is extensively fractured and
433 moderately crushed, which has collapsed some of the internal trabeculae (Fig. 7).
434 Despite this damage, it is clear that the medullary cavity was not open, and that
435 trabeculae extended throughout the medullary region. Cortical thickness is relatively
436 high (~50%) in some regions, but varies around the cortex.

437 Most of the cortex is heavily remodelled, resulting in dense Haversian bone
438 (Francillon-Vieillot *et al.* 1990), and combined with expansion of the medullary cavity
439 this feature has obscured all primary bone in the inner cortex. The trabeculae of the
440 medullary cavity are formed of lamellar bone (Francillon-Vieillot *et al.* 1990) with
441 flattened osteocyte lacunae (Fig. 8D). Within the medullary spaces, linings of
442 endosteally-derived lamellar bone (Bromage *et al.* 2009) are apparent. The size of
443 the medullary spaces decreases periosteally (Fig. 7B), and close to the cortex, some
444 of the medullary spaces resemble large secondary osteons (Fig. 7A). There is a
445 stark transition between the zone of dense Haversian bone and the trabeculae of the
446 medullary cavity. **At this transition, the diameter of vascular spaces decreases
447 significantly and no endosteal lamellar bone is visible between the secondary
448 osteons. The zone of dense Haversian bone is defined here as the region where**

449 secondary remodelling completely obscures any intervening primary tissue.
450 Secondary osteons within the zone of dense Haversian bone are longitudinally
451 oriented and decrease in size periosteally (Fig. 7A). Endosteally, several overlapping
452 generations of secondary osteons can be discerned, and in some areas there are **at**
453 **least three and maybe four generations of secondary osteons** (Fig. 8C). The density
454 of secondary remodelling decreases periosteally, so that there are fewer overlapping
455 secondary osteons, and more primary bone is visible between them (Fig. 7D). **We**
456 **interpret this zone as more representative of abundant secondary remodelling rather**
457 **than true dense Haversian bone, because primary tissue is visible between the**
458 **secondary osteons.**

459 In the thickest part of the cortex an extensive area of primary bone is
460 preserved towards the periosteal surface (Fig. 7C). This primary bone is fibrolamellar
461 with a relatively sparse osteocyte lacunae ($\sim 14500/\text{mm}^3$). Osteocyte lacunae are
462 lenticular where they surround primary osteons, but are denser and more globose in
463 the intermittent areas of woven bone (Fig. 8A). The primary bone is relatively **poorly**
464 vascularized (Fig. 7C) compared to most dinosaurs (Horner *et al.* 1999; Horner &
465 Padian 2004; Padian *et al.* 2004; Sander *et al.* 2011; Woodward *et al.* 2015), and the
466 density, orientation, and size of vascular canals varies throughout the cortex. In most
467 areas, vasculature is longitudinal in orientation, and these canals are randomly
468 dispersed rather than arranged into circumferential rings (Fig. 7C). Several areas
469 have a higher proportion of anastomosing canals and thus exhibit reticular
470 vascularity, but these are confined to small, randomly distributed patches rather than
471 continuous layers or zones (Fig. 7C). The diameter of the longitudinal vascular
472 canals varies randomly from $\sim 20\ \mu\text{m}$ to $\sim 100\ \mu\text{m}$, and even adjacent canals can be
473 considerably different in size. Vascularity is consistent in density and orientation
474 approaching the periosteal surface, and numerous vascular canals are open to the
475 periosteal surface (Fig. 7C, D, 8F). One line of arrested growth, or LAG, is visible in
476 the primary bone of the cortex, just periosteal to the zone of Haversian bone (Fig.
477 7D). There are no LAGs near the periosteal surface, nor is there development of an
478 external fundamental system (Horner *et al.* 1999; Woodward *et al.* 2011, 2015).

479 A region of secondary remodelling is present within the primary cortical bone,
480 about one third of the distance from the zone of dense Haversian bone to the
481 periosteal surface, approximately 0.5–1 mm external to the LAG (Fig. 7D). This
482 region is separated from the Haversian bone by a band of primary fibrolamellar bone
483 (Fig. 7D) with small, longitudinally oriented canals, where the LAG is situated (Fig.
484 8B). The secondary osteons in the zone of remodelling are generally larger than
485 those in the periosteal portion of the Haversian zone, and are more comparable in
486 size to those nearer the medullary cavity. The secondary osteons in the zone of
487 remodelling frequently interconnect, which creates a reticular pattern of vascularity
488 overall (Fig. 7D). No cross-cutting of the secondary osteons can be detected, in
489 contrast with the zone of Haversian bone. Where the primary bone is visible between
490 the secondary osteons in this region of secondary remodelling, some erosive cavities
491 can be discerned (Fig. 8E). These can be differentiated from primary osteons by

492 their scalloped edges, created by Howship's lacunae, which are evidence of
493 resorption by osteoclasts (Francillon-Vieillot *et al.* 1990).

494 Assuming NMS.Eigg.2017 is a hind limb bone, the bone matrix and internal
495 structure exclude certain identifications. Fibrolamellar bone is known only in
496 amniotes (Francillon-Vieillot *et al.* 1990), specifically in synapsids (Chinsamy-Turan
497 2012), some marine reptiles (de Buffr enil & Mazin 1990; Klein 2010; Kolb *et al.* 2011;
498 Houssaye *et al.* 2014; Klein *et al.* 2015; Wintrich *et al.* 2017), and archosaurs
499 (Horner *et al.* 2001; de Ricql es *et al.* 2003; Padian *et al.* 2004). The large size of the
500 bone precludes a synapsid identification, while the lack of highly porous
501 (osteoporotic), or compacted (pachyostotic) bone rules out marine reptiles, which
502 have these features as adaptations for a marine lifestyle (Houssaye 2009; Houssaye
503 *et al.* 2014). Additionally, the cortical thickness of NMS.Eigg.2017 is greater than
504 would be expected of pelagic animals like ichthyosaurs.

505 The histology of NMS.Eigg.2017 is most similar to that of dinosaurs, which
506 typically have highly vascularized fibrolamellar **zonal** bone with LAGs (Horner *et al.*
507 1999; Padian *et al.* 2004; Padian & Lamm 2013). In contrast, crocodylomorphs and
508 pseudosuchians more commonly show lamellar-zonal bone with lower vascularity
509 and less fibrolamellar tissue (de Ricql es *et al.* 2003; Andrade & Say o 2014; Say o
510 *et al.* 2016; Cubo *et al.* 2017), whereas pterosaurs have extensive medullary cavities
511 with extremely thin cortical walls (De Ricql es *et al.* 2000; Padian *et al.* 2004)

512 Detailed comparative anatomy suggests that NMS.Eigg.2017 is most likely to
513 be either a thyreophoran or sauropod fibula. The distinctive combination of
514 osteohistological features in NMS.Eigg.2017 provides further clues, but uncertainty
515 over the identity of the element makes the significance of certain features—like
516 vascular orientation—unclear. Different bones of the same individual, and even
517 different regions within the same bone, can produce markedly different histological
518 signatures (Horner *et al.* 1999; Cullen *et al.* 2014; Woodward *et al.* 2014; Nacarino-
519 Meneses *et al.* 2016). Smaller bones tend to grow at slower rates and may
520 experience more rapid secondary remodelling (Horner *et al.* 1999), **and fibulae**
521 **especially tend to show more remodelling. The pervasive remodelling in**
522 **NMS.Eigg.2017 may therefore be the result of the element rather than taxonomic**
523 **identity.** However, as NMS.Eigg.2017 likely represents a large hind limb bone, its
524 histology probably generally reflects the overall growth of the individual **rather than**
525 **solely exhibiting a biomechanical signal.**

526 The microstructure of NMS.Eigg.2017 differs from theropod limb bones in that
527 the medullary cavity is not hollow (Chinsamy, 1990; Horner & Padian 2004; Bybee *et al.*
528 2006; Lee & O'Connor 2013; Cullen *et al.* 2014). **In theropods, some sparse**
529 **trabeculae can be present in the medullary cavity where the diaphysis grades into**
530 **the metaphysis. However, it is unlikely that the closed medullary cavity in**
531 **NMS.Eigg.2017 is attributable to this phenomenon, because trabeculae completely**
532 **fill the medullary cavity, and because the section was taken relatively close to the**
533 **midshaft (Fig. 2).** Sauropod osteohistology is well studied, and their limb bone
534 cortices are characterized by a laminar vascular arrangement indicative of rapid
535 growth (Sander 2000, 2004; Klein & Sander 2008; Woodward & Lehman 2009;

536 Sander *et al.* 2011a and b), even in smaller forms (Sander *et al.* 2006; Stein *et al.*
537 2010). This arrangement is not the case in NMS.Eigg.2017, where vasculature is
538 arranged randomly rather than into circumferential rows (Fig. 7C). Neosauropods
539 tend to lack distinct LAGs (Sander *et al.* 2011), and in many cases growth marks are
540 preserved instead as polish lines visible in reflected light (de Ricqlès 1983). The
541 presence of a LAG in NMS.Eigg.2017 therefore argues against a neosauropod
542 affinity for the specimen. The low osteocyte lacunar density of NMS.Eigg.2017 is
543 further evidence against a sauropod affinity, as sauropods typically have much
544 denser osteocyte lacunae than other comparably-sized animals (Stein & Werner
545 2013).

546 Of the possible dinosaur groups, the histology of NMS.Eigg.2017 is most
547 similar to that of thyreophoran dinosaurs. The combination of predominantly
548 longitudinal vascularity indicative of a relatively low growth rate and abundant
549 secondary remodelling is seen in this group (Hayashi *et al.* 2009; Redelstorff &
550 Sander 2009; Redelstorff *et al.* 2013; Stein *et al.* 2013; Maidment *et al.* 2018). Most
551 osteohistological work on thyreophorans has focused on their osteoderms (e.g.
552 Hayashi *et al.* 2009; Burns & Currie 2014; Horner *et al.* 2016), but a few studies have
553 sampled long bones. In a review of ankylosaur osteohistology, Stein *et al.* (2013)
554 noted abundant structural fibres within the primary and secondary bone of the limb
555 elements of derived North American ankylosaurs. In contrast, stegosaurs lack
556 structural fibres and have slightly less—but still abundant—secondary remodelling at
557 equivalent ontogenetic stages (Hayashi *et al.* 2009; Redelstorff & Sander 2009;
558 Redelstorff *et al.* 2013; Stein *et al.* 2013). Hayashi *et al.* (2009) sampled fibulae from
559 an ontogenetic sequence of *Stegosaurus*, and Maidment *et al.* (2018) sampled a
560 fibula of the stegosaur *Hesperosaurus*. Both showed that vasculature in medium to
561 large sized individuals was predominantly longitudinal with extensive secondary
562 remodelling and the development of LAGs.

563 The histology of NMS.Eigg.2017 is remarkably similar to the medium to large-
564 sized *Stegosaurus* fibulae described by Hayashi *et al.* (2009), except that an external
565 fundamental system is not developed. This difference could be explained by a
566 slightly younger ontogenetic stage in NMS.Eigg.2017, as the external fundamental
567 system is only developed late in life (Horner *et al.* 1999; Woodward *et al.* 2011,
568 2015). In this aspect, NMS.Eigg.2017 is more like the fibula of *Hesperosaurus* MOR
569 9728 described by Maidment *et al.* (2018), which also lacks an external fundamental
570 system. The two specimens are virtually identical in cross-sectional shape, and
571 although the cortical thickness of MOR 9728 is greater than NMS.Eigg.2017, this
572 could be because the samples were taken at different locations of the midshaft.
573 MOR 9728 is more extensively remodelled than NMS.Eigg.2017, but where primary
574 bone remains near the periosteal surface, the vasculature is sparse and
575 longitudinally oriented, as in NMS.Eigg.2017.

576 The osteohistological signal of slow growth with extensive remodelling is
577 evident in *Kentrosaurus*. Based on the femora, *Kentrosaurus* had a slightly faster
578 growth rate than *Stegosaurus* or NMS.Eigg.2017, but still lower than other
579 comparably sized ornithischians (Redelstorff & Sander 2009; Redelstorff *et al.* 2013).

580 NMS.Eigg.2017 shares with stegosaurs the abundant secondary remodelling (Fig.
581 7A, 2C), randomly arranged longitudinal–reticular vasculature (Fig. 7C), and the
582 absence of the structural fibres, as present in ankylosaurs. Of the dinosaurian
583 candidates, the histology of NMS.Eigg.2017 is therefore most consistent with
584 stegosaurs.

585 The fibrolamellar bone matrix of NMS.Eigg.2017 is indicative of relatively high
586 growth rates compared to more basal tetrapods (Francillon-Vieillot *et al.* 1990;
587 Castanet *et al.* 2000; Padian & Lamm 2013). Based on the vascular canals within the
588 primary cortical bone, the predominantly longitudinal vascularity with small regions of
589 reticular vascularity suggests however that growth in this element was on the low
590 end of the spectrum of fibrolamellar growth rates (Castanet *et al.* 2000; de Margerie
591 2004). Vascularity at the periosteal surface and the absence of an external
592 fundamental system also suggest this animal was actively growing at the time of
593 death (Horner *et al.* 1999; Woodward *et al.* 2011, 2015). The position of the single
594 LAG towards the middle of the cortex indicates considerable growth in the last year
595 of life. The consistent density and orientation of vascularity in the periosteal portion
596 of the cortex suggests that growth had not slowed, and that NMS.Eigg.2017 was in
597 the maximum growth phase of its life when it died (Lee *et al.* 2013).

598 Establishing the chronological age of NMS.Eigg.2017 is difficult because of
599 the extensive secondary remodelling of the cortex and expansion of the medullary
600 cavity. The combination of active growth and extensive secondary remodelling is
601 unusual, as these typically characterise different phases of growth (Klein and Sander
602 2008; Padian & Lamm 2013). Secondary remodelling usually progresses from the
603 inner cortex outwards (Mitchell & Sander 2014), and therefore Haversian bone in the
604 outer cortex only occurs later in life (Kerley 1965; Klein & Sander 2008). However, it
605 can be induced by biomechanical stress or other environmental factors (Padian &
606 Lamm 2013), which may explain the abundance of secondary osteons in conjunction
607 with high growth rates. It is clear from the single LAG that this individual was at least
608 one year old at the time of death, but it was almost certainly considerably older. The
609 abundance of secondary remodelling and overlapping generations of secondary
610 osteons are typically associated with advanced age (Kerley 1965; Uytterschaut
611 1993; Horner *et al.* 1999; Klein & Sander 2008; Sander *et al.* 2011). Unfortunately,
612 retrocalculation of growth marks is not possible with only a single LAG (Cooper *et al.*
613 2008; Lee *et al.* 2013), so the exact age of NMS.Eigg.2017 at death cannot be
614 determined.

615

616

617 **6. Conclusion**

618

619 This specimen, NMS.Eigg.2017, is the first unequivocal dinosaur fossil found in
620 Scotland outside of Skye. Identification of damaged isolated bones can be
621 challenging, but finding ways to approach such identification is especially relevant for
622 the dinosaur fossil record in Scotland, which comprises relatively incomplete material
623 compared to contemporaneous sites in England.

624 Through detailed anatomical comparison, we find the overall proportions and
625 cross-sectional geometry similar to the fibulae of thyreophorans. The length to width
626 ratio, and certain features such as a longitudinal ridge are similar to features present
627 in a sauropod fibula, and NMS.Eigg.2017 bears resemblance to the fibula of juvenile
628 *Cetiosaurus*. However, examination of the microstructure of the bone through
629 histological analysis reveals a combination of predominantly longitudinal vascularity
630 indicative of a relatively low growth rate, with abundant secondary remodelling—both
631 strongly indicative of thyreophoran (particularly stegosaur) limb bone microstructure.
632 The vascularity at the periosteal surface and absence of an external fundamental
633 system indicate it belonged to a juvenile animal still rapidly growing at the time of
634 death. We therefore consider NMS.Eigg.2017 most likely to represent a juvenile
635 stegosaur fibula.

636 The presence of a thyreophoran bone on the Isle of Eigg adds a significant
637 new datapoint for dinosaur distribution in the Middle Jurassic. The dinosaur body
638 fossil record is sparse in Scotland, and this specimen provides evidence for a large-
639 bodied animal in a locality previously not known for dinosaur fossils. Weathering,
640 tooth marks and a layer of small molluscs on the underside of the femur suggest
641 transport and scavenging of the carcass prior to deposition, which is consistent with
642 its entombment in the fluvio-deltaic Valtos Sandstone Formation.

643 This specimen increases the palaeontological significance of the Isle of Eigg.
644 The island is already well known for the fossiliferous 'Hugh Miller Reptile Bed' (Miller
645 1858; Hudson 1966; Benton 1995), and for the distinctive features of its geological
646 landscape, such as the Sgurr of Eigg. Although a theropod tooth fragment from Eigg
647 was mentioned by Rees and Underwood (2005), it has subsequently been lost and
648 this cannot be confirmed. This makes NMS.Eigg.2017 the first unequivocal dinosaur
649 specimen from the island.

650 This discovery hints that continued exploration of the Valtos Sandstone
651 Formation - and other parts of the Great Estuarine Group - could yield further vital
652 fossil material. These finds would undoubtedly continue to enrich our picture of
653 ecosystem diversity in Middle Jurassic Scotland.

654

655

656 **8. Acknowledgements**

657

658 We would like to thank the Eigg Community Trust, Maggie Fyffe, Craig Lovatt, and
659 people of Eigg for permitting us access and for supporting our work on their beautiful
660 island, and Scottish Natural Heritage (including Sarah McGroary and Colin
661 MacFadyen) for permits and logistical support. We thank Western Isles Ferries and
662 Alastair Kirk for helping to collect and transport the bone. Thanks go to Roger
663 Benson for providing images of specimens. Our research was funded by a National
664 Geographic Grant GEFNE185-16 awarded to SLB. Histological work was funded
665 primarily by a Newton International Fellowship to GFF and partially by a Philip
666 Leverhulme Prize to SLB and the School of Geosciences, University of Edinburgh.
667 Authors TC to MW are listed alphabetically for their equal contribution to fieldwork

668 and to this manuscript. We also thank our two anonymous reviewers for their helpful
669 and constructive comments, which improved this manuscript.

670
671

672 9. References

673

674 Allain, R. & Aquesbi, N. 2008. Anatomy and phylogenetic relationships of
675 *Tazoudasaurus naimi* (Dinosauria, Sauropoda) from the late Early Jurassic of
676 Morocco. *Geodiversitas* **30**, 345–424.

677

678 de Andrade, R. C. L. P. & Sayão, J. M. 2014. Paleohistology and Lifestyle Inferences
679 of a Dyrosaurid (Archosauria: Crocodylomorpha) from Paraíba Basin (Northeastern
680 Brazil). *PLoS ONE* **9**, e102189.

681

682 Andrews, C. W. 1910. *A Descriptive Catalogue of the Marine Reptiles of the Oxford*
683 *Clay, Part One*. British Museum (Natural History), London.

684

685 Andrews, C. W. 1913. *A Descriptive Catalogue of the Marine Reptiles of the Oxford*
686 *Clay, Part Two*. British Museum (Natural History), London.

687

688 Andrews, J. E. 1985. The sedimentary facies of a late Bathonian regressive episode:
689 the Kilmaluag and Skidiburgh Formations of the Great Estuarine Group, Inner
690 Hebrides, Scotland. *Journal of the Geological Society London* **142**, 1119–1137.

691

692 Andrews, J. E. & Hudson, J. D. 1984. First Jurassic dinosaur footprint from Scotland.
693 *Scottish Journal of Geology* **20**, 129–134.

694

695 Anquetin, J., Barrett, P. M., Jones, M. E. H., Moore-Fay, S. & Evans, S. E. 2009. A
696 new stem turtle from the Middle Jurassic of Scotland: new insights into the evolution
697 and palaeoecology of basal turtles. *Proceedings of the Royal Society B* **276**, 879–
698 886.

699

700 Anquetin, J. 2009. A new stem turtle from the Middle Jurassic of Scotland: new
701 insights into the evolution and palaeoecology of basal turtles. *Proceedings of the*
702 *Royal Society B* **276**, 879–886.

703

704 Anquetin, J. 2010. The anatomy of the basal turtle *Eileanchelys waldmani* from the
705 Middle Jurassic of the Isle of Skye, Scotland. *Earth and Environmental Science*
706 *Transactions of the Royal Society of Edinburgh* **101**, 67–96.

707

708 Arkell, W. J. 1933. *The Jurassic System in Great Britain*. Oxford University Press,
709 Oxford.

710

- 711 Bandyopadhyay, S., Gillette, D. D., Ray, S. & Sengupta, D. P. 2010. Osteology of
712 *Barapasaurus tagorei* (Dinosauria: Sauropoda) from the early Jurassic of India.
713 *Palaeontology* **53**, 533–569.
- 714
- 715 Barrett, P. M. 2006. A sauropod dinosaur tooth from the Middle Jurassic of Skye,
716 Scotland. *Transactions of the Royal Society of Edinburgh: Earth Sciences* **97**, 25–29.
- 717
- 718 Barrett, P. M. & Maidment, S. C. R. 2017. The evolution of ornithischian
719 quadrupedality. *Journal of Iberian Earth Sciences* **43**, 463–477.
- 720
- 721 Barron, A. J. M., Lott, G. K. & Riding, J. B. 2012. Stratigraphic Framework for the
722 Middle Jurassic Strata of Great Britain and the Adjoining Continental Shelf: Research
723 Report RR/11/06. British Geological Survey, Keyworth. 177 pp.
- 724
- 725 Benson, R. B. J. 2010. A description of *Megalosaurus bucklandii* (Dinosauria:
726 Theropoda) from the Bathonian of the UK and the relationships of Middle Jurassic
727 theropods. *Zoological Journal of the Linnean Society* **158**, 882–935.
- 728
- 729 Benson, R. B. J. 2013. *Marine Reptiles*. In MacLeod, N., Archibald, J. D., & Levin, P.
730 (eds) *Grzimek's Animal Life Encyclopedia, Extinction*, 267–279. Farmington Hills,
731 Michigan: Gale Cengage Learning.
- 732
- 733 Benson, R. B. J., Campione, N. E., Carrano, M. T., Mannion, P. D., Sullivan, C.,
734 Upchurch, P. & Evans, D. C. 2014. Rates of dinosaur body mass evolution indicate
735 170 million years of sustained ecological innovation on the avian lineage. *PLoS*
736 *Biology* **12**, e1001853.
- 737
- 738 Bertozzo, F., Dalla Vecchia, F. M. & Fabbri, M. 2017. The Venice specimen of
739 *Ouranosaurus nigeriensis* (Dinosauria, Ornithopoda). *PeerJ* **5**, e3403.
- 740
- 741 Boneham, B. F. W. & Forsey, G. F. 1992. Earliest stegosaur dinosaur. *Terra Nova* **4**,
742 628–632.
- 743
- 744 Bromage, T. G., Lacruz, R. S., Hogg, R., Goldman, H. M., McFarlin, S. C., Warshaw,
745 J., Dirks, W., Perez-Ochoa, A., Smolyar, I., Enlow, D. H. & Boyde, A. 2009. Lamellar
746 Bone is an Incremental Tissue Reconciling Enamel Rhythms, Body Size, and
747 Organismal Life History. *Calcified Tissue International* **84**, 388–404.
- 748
- 749 de Buffrénil, V. & Mazin, J. -M. 1990. Bone histology of the ichthyosaurs:
750 comparative data and functional interpretation. *Paleobiology* **16**, 435–447.
- 751
- 752 Burns, M. E. & Currie, P. J. 2014. External and internal structure of ankylosaur
753 (Dinosauria, Ornithischia) osteoderms and their systematic relevance. *Journal of*
754 *Vertebrate Paleontology* **34**, 835–851.

- 755
756 Bybee, P. J., Lee, A. H. & Lamm, E. -T. 2006. Sizing the Jurassic theropod dinosaur
757 *Allosaurus*: Assessing growth strategy and evolution of ontogenetic scaling of limbs.
758 *Journal of Morphology* **267**, 347–359.
759
- 760 Castanet, J., Rogers, K. C. Cubo, J. & Jacques-Boisard, J. 2000. Periosteal bone
761 growth rates in extant ratites (ostriche and emu). Implications for assessing growth in
762 dinosaurs. *Comptes Rendus de l'Académie Des Sciences-Series III-Sciences de La*
763 *Vie* **323**, 543–550.
764
- 765 Cerda, I. A. & Chinsamy, A. 2012. Biological implications of the bone microstructure
766 of the Late Cretaceous Ornithopod Dinosaur *Gasparinisaura cincosaltensis*. *Journal*
767 *of Vertebrate Paleontology* **32**, 355–368.
768
- 769 Chinsamy, A. 1990. Physiological implications of the bone histology of *Syntarsus*
770 *rhodesiensis* (Saurischia: Theropoda). *Paleontologica Africana* **27**, 77–82.
771
- 772 Clark, N. D. L. 2001. A thyreophoran dinosaur from the early Bajocian (Middle
773 Jurassic) of the Isle of Skye, Scotland. *Scottish Journal of Earth Sciences* **37**, 19–26.
774
- 775 Clark, N. D. L. 2018. Review of the dinosaur remains from the Middle Jurassic of
776 Scotland, UK. *Geosciences*, **8**, 53.
777
- 778 Clark, N. D. L. & Barco-Rodriguez, J. L. 1998. The first dinosaur trackway from the
779 Valtos Sandstone Formation (Bathonian, Jurassic) of the Isle of Skye, Scotland, UK.
780 *Geogaceta* **24**, 79–82.
781
- 782 Clark, N. D. L. & Brett-Surman, M. K. 2008. A comparison between dinosaur
783 footprints from the Middle Jurassic of the Isle of Skye, Scotland, UK, and Shell,
784 Wyoming, USA. *Scottish Journal of Geology* **44**, 139–150.
785
- 786 Clark, N. D. L. & Gavin, P. 2016. New Bathonian (Middle Jurassic) sauropod remains
787 from the Valtos Sandstone Formation, Isle of Skye, Scotland. *Scottish Journal of*
788 *Geology* **52**, 71–75.
789
- 790 Clark, N. D. L., Nimmo, F. & Nicholas, C. J. 1993. A new occurrence of Scottish
791 plesiosauran remains from the Isle of Skye. *Scottish Journal of Geology* **29**, 197–
792 199.
793
- 794 Clark, N. D. L., Boyd, J. D., Dixon, R. J. & Ross, D. A. 1995. The first Middle Jurassic
795 dinosaur from Scotland: a cetiosaurid? (Sauropoda) from the Bathonian of the Isle of
796 Skye. *Scottish Journal of Geology* **31**, 171–176.
797

- 798 Clark, N. D. L., Booth, P., Booth, C. & Ross, D. A. 2004. Dinosaur footprints from the
799 Duntulm Formation (Bathonian, Jurassic) of the Isle of Skye. *Scottish Journal of*
800 *Geology* **40**, 13–21.
- 801
- 802 Clark, N. D. L., Ross, D. A. & Booth, P. 2005. Dinosaur tracks from the Kilmaluag
803 Formation (Bathonian, Middle Jurassic) of Score Bay, Isle of Skye, Scotland, UK.
804 *Ichnos* **12**, 93–104.
- 805
- 806 Cooper, L. N., Lee, A. H. Taper, M. L. & Horner, J. R. 2008. Relative growth rates of
807 predator and prey dinosaurs reflect effects of predation. *Proceedings of the Royal*
808 *Society B: Biological Sciences* **275**, 2609–2615.
- 809
- 810 Cubo, J., Köhler, M. & de Buffrénil, V. 2017. Bone histology of *Iberosuchus*
811 *macrodon* (Sebecosuchia, Crocodylomorpha). *Lethaia* **50**, 495–503.
- 812
- 813 Cullen, T. M., Evans, D. C., Ryan, M. J., Currie, P. J. & Kobayashi, Y. 2014.
814 Osteohistological variation in growth marks and osteocyte lacunar density in a
815 theropod dinosaur (Coelurosauria: Ornithomimidae). *BMC Evolutionary Biology* **14**,
816 231.
- 817
- 818 dePolo, P. E., Brusatte, S. L., Challands, T. J., Foffa, D., Ross, D. A., Wilkinson, M.
819 & Yi, H. Y. 2018. A sauropod-dominated tracksite from Rubha nam Brathairean
820 (Brothers' Point), Isle of Skye, Scotland. *Scottish Journal of Geology* **54**, 1–12.
- 821
- 822 dePolo, P. E., Brusatte, S. L., Challands, T. J., Foffa, D., Wilkinson, M., Clark, N. D.
823 L., Hoad, J., da Pereira, P. V. L. G., Ross, D. A. & Wade, T. J. 2020. Novel track
824 morphotypes from new tracksites indicate increased Middle Jurassic dinosaur
825 diversity on the Isle of Skye, Scotland. *PlosONE* [online]
- 826
- 827 Evans, S., Barrett, P., Hilton, J., Butler R. J., Jones, M. E. H., Liang, M. -M., Parrish,
828 J. C., Rayfield, E. J., Sigogneau-Russell, D. & Underwood, C. J. 2006. The Middle
829 Jurassic vertebrate assemblage of Skye, Scotland. In Barrett, P. & Evans, S. (eds)
830 *Proceedings of the Ninth Symposium on Mesozoic Terrestrial Ecosystems and Biota*,
831 36–39. London: Natural History Museum.
- 832
- 833 Foffa, D., Johnson, M. M., Young, M. T., Steel, L., Brusatte, S. L. 2019. Revision of
834 the Late Jurassic deep-water teleosauroid crocodylomorph *Teleosaurus megarhinus*
835 Hulke, 1871 and evidence of pelagic adaptations in Teleosauroidea. *PeerJ* **7**, e6646.
- 836
- 837 Francillon-Vieillot, H., de Buffrenil, V. Castanet, J. Gkraudie, J. Meunier, F. J. Sire, J.
838 Y. Zylberberg, L. & de Ricqlès, A. J. 1990. Microstructure and Mineralization of
839 Vertebrate Skeletal Tissues. In Carter J. G. (ed.) *Skeletal Biomineralization:*
840 *Patterns, Processes, and Evolutionary Trends*, 471–530. New York: Van Nostrand
841 Reinhold.

- 842
843 Galton, P. M. 1983. *Sarcolestes leedsi* Lydekker, an ankylosaurian dinosaur from the
844 Middle Jurassic of England. *Neues Jahrbuch für Geologie und Paläontologie*
845 *Monatshefte* **3**, 141–155.
- 846
847 Galton, P. M. 1985. British plated dinosaurs (Ornithischia: Stegosauria). *Journal of*
848 *Vertebrate Paleontology* **11**, 211–254.
- 849
850 Galton, P. M. & Upchurch, P. 2004. Stegosauria. In Weishampel, D.B., Dodson, P. &
851 Osmólska, H. (eds) *The Dinosauria* (second edition), 343–362. Berkeley, USA:
852 University of California Press.
- 853
854 Harris, J. P. & Hudson, J. D. 1980. Lithostratigraphy of the Great Estuarine Group
855 (Middle Jurassic), Inner Hebrides. *Scottish Journal of Geology* **16**, 231–250.
- 856
857 Hayashi, S., Carpenter, K. & Suzuki, D. 2009. Different growth patterns between the
858 skeleton and osteoderms of *Stegosaurus* (Ornithischia: Thyreophora). *Journal of*
859 *Vertebrate Paleontology* **29**, 123–131.
- 860
861 Hendrickx, C., Hartman, S. A. & Mateus, O. 2015. An overview of non-avian
862 theropod discoveries and classification. *PalArch's Journal of Vertebrate*
863 *Palaeontology* **12**, 1–73.
- 864
865 Holwerda, F. M. & Pol, D. 2018. Phylogenetic analysis of Gondwanan basal
866 eusauropods from the Early-Middle Jurassic of Patagonia, Argentina. *Spanish*
867 *Journal of Palaeontology* **33**, 298–298.
- 868
869 Holwerda, F. M., Rauhut, O. W. M. & Pol, D. 2020. Osteological revision of the
870 holotype of the Middle Jurassic sauropod dinosaur *Patagosaurus fariasi* (Sauropoda:
871 Cetiosauridae) BONAPARTE 1979. *Geodiversitas* (in press).
- 872
873 Horner, J. R., & K. Padian. 2004. Age and growth dynamics of *Tyrannosaurus rex*.
874 *Proceedings of the Royal Society B: Biological Sciences* **271**, 1875–1880.
- 875
876 Horner, J. R., A. de Ricqlès, & K. Padian. 1999. Variation in dinosaur
877 skeletochronology indicators: implications for age assessment and physiology.
878 *Paleobiology* **25**, 295–304.
- 879
880 Horner, J. R., K. Padian, & A. de Ricqlès. 2001. Comparative osteohistology of some
881 embryonic and perinatal archosaurs: developmental and behavioral implications for
882 dinosaurs. *Paleobiology* **27**, 39–58.
- 883

- 884 Horner, J. R., H. N. Woodward, & A. M. Bailleul. 2016. Mineralized tissues in
885 dinosaurs interpreted as having formed through metaplasia: A preliminary
886 evaluation. *Comptes Rendus Palevol* **15**, 176–196.
- 887
- 888 Horner, J. R., De Ricqlès, A., Padian, K. & Scheetz, R. D. 2009. Comparative long
889 bone histology and growth of the “hypsilophodontid” dinosaurs *Orodromeus makelai*,
890 *Dryosaurus altus*, and *Tenontosaurus tilletii* (Ornithischia: Euornithopoda). *Journal*
891 *of Vertebrate Paleontology* **29**, 734–747.
- 892
- 893 Houssaye, A. 2009. “Pachyostosis” in aquatic amniotes: a review. *Integrative*
894 *Zoology* **4**, 325–340.
- 895
- 896 Houssaye, A. 2013. Bone Histology of Aquatic Reptiles. *Biological Journal of the*
897 *Linnean Society of London* **108**, 3–21.
- 898
- 899 Houssaye, A., T. M., Scheyer, C., Kolb, V., Fischer, & Sander, P. M. 2014. A New
900 Look at Ichthyosaur Long Bone Microanatomy and Histology: Implications for Their
901 Adaptation to an Aquatic Life. *PLoS ONE* **9**, e95637.
- 902
- 903 Hua, S. 1999. Le crocodylien *Machimosaurus mosae* (Thalattosuchia,
904 Teleosauridae) du Kimmeridgien du Boulonnais (Pas de Calais, France).
905 *Palaeontographica Abteilung A* **252**, 141–170.
- 906
- 907 Hua, S., & De Buffrenil, V. 1996. Bone Histology as a Clue in the Interpretation of
908 Functional Adaptations in the Thalattosuchia (Reptilia, Crocodylia). *Journal of*
909 *Vertebrate Paleontology* **16**, 703–717.
- 910
- 911 Hübner, T. R. 2012. Bone Histology in *Dysalotosaurus lettowvorbecki* (Ornithischia:
912 Iguanodontia) – Variation, Growth, and Implications. *PLoS ONE* **7**, e29958.
- 913
- 914 Hudson, J. D. 1962. The stratigraphy of the Great Estuarine Series (Middle Jurassic)
915 of the Inner Hebrides. *Transactions of the Edinburgh Geological Society* **19**, 139–
916 165.
- 917
- 918 -- 1963. The ecology and stratigraphical distribution of the invertebrate fauna of the
919 Great Estuarine Series. *Palaeontology* **6**, 327–34.
- 920
- 921 -- 1966. Hugh Miller's Reptile Bed and the Mytilus Shales, Middle Jurassic, Isle of
922 Eigg, Scotland. *Scottish Journal of Geology* **2**, 265–281.
- 923
- 924 Hudson, J. D. & Harris, J. P. 1979. Sedimentology of the Great Estuarine Group
925 (Middle Jurassic) of north-west Scotland. *Symposium sur la Sédimentation de*
926 *Jurassique Ouest Européen, Paris, 9-10 May 1977. Association des*
927 *Sédimentologues Français, Publication Speciale Vol. 1*, 1–13.

928

929 Johnson, M. M., Young, M. T., Steel, L., Foffa, D., Smith, A. S., Hua, S., Havlik, P.,
930 Howlett, E.A. & Dyke, G. 2017. Re-description of ‘*Steneosaurus*’ *obtusidens*
931 Andrews, 1909), an unusual macrophagous teleosaurid crocodylomorph from the
932 Middle Jurassic of England. *Zoological Journal of the Linnean Society* **1**, 1–34.

933

934 Kerley, E. R. 1965. The microscopic determination of age in human bone. *American*
935 *Journal of Physical Anthropology* **23**, 149–163.

936

937 Klein, N. 2010. Long Bone Histology of Sauropterygia from the Lower Muschelkalk of
938 the Germanic Basin Provides Unexpected Implications for Phylogeny. *PLoS ONE* **5**,
939 e11613.

940

941 Klein, N., & M. Sander. 2008. Ontogenetic stages in the long bone histology of
942 sauropod dinosaurs. *Paleobiology* 34:247–263.

943

944 Klein, N., Houssaye, A., Neenan, J. M. & Scheyer, T. M. 2015. Long bone histology
945 and microanatomy of Placodontia (Diapsida: Sauropterygia). *Contributions to*
946 *Zoology* **84**, 59–S15.

947

948 Kolb, C., Sánchez-Villagra, M. R. & Scheyer T. M. 2011. The palaeohistology of the
949 basal ichthyosaur *Mixosaurus* (Ichthyopterygia, Mixosauridae) from the Middle
950 Triassic: Palaeobiological implications. *Comptes Rendus Palevol* **10**, 403–411.

951

952 Lamm, E. -T. 2013. Preparation and Sectioning of Specimens. In Padian, K. &
953 Lamm, E. -T. (eds) *Bone Histology of Fossil Tetrapods: Advancing Methods,*
954 *Analysis, and Interpretation*, 55–160. Berkeley, USA: University of California Press.

955

956 Lee, G.W. & Buckman, S. S. 1920. *The Mesozoic Rocks of Applecross, Raasay, and*
957 *North-East Skye*. Memoirs of the Geological Survey, Scotland, Edinburgh.

958

959 Lee, A. H. & O’Connor, P. M. 2013. Bone histology confirms determinate growth and
960 small body size in the noasaurid theropod *Masiakasaurus knopfleri*. *Journal of*
961 *Vertebrate Paleontology* **33**, 865–876.

962

963 Lee, A. H., Huttenlocker, A. K., Padian, K. & Woodward, H. N. 2013. Analysis of
964 growth rates. In Padian, K. & Lamm, E. -T. (eds) *Bone Histology of Fossil Tetrapods:*
965 *Advancing Methods, Analysis, and Interpretation*. Berkeley, USA: University of
966 California Press.

967

968 Liston, J. J. 2004. A re-examination of a Middle Jurassic sauropod limb bone from
969 the Bathonian of the Isle of Skye. *Scottish Journal of Geology* **40**, 119–122.

970

- 971 Maidment, S. C. R., Woodruff, D. C., & Horner, J. R. 2018. A new specimen of the
972 ornithischian dinosaur *Hesperosaurus mjosi* from the Upper Jurassic Morrison
973 Formation of Montana, U.S.A., and implications for growth and size in Morrison
974 stegosaurs. *Journal of Vertebrate Paleontology* **38**, p.e1406366.
975
- 976 Mannion, P. D., Benson, R. B. J., Carrano, M. T., Tennant, J. P., Judd, J. & Butler,
977 R. J. 2015. Climate constrains the evolutionary history and bio-diversity of
978 crocodylians. *Nature Communications* **6**, 8438.
979
- 980 de Margerie, E. 2004. Assessing a relationship between bone microstructure and
981 growth rate: a fluorescent labelling study in the king penguin chick (*Aptenodytes*
982 *patagonicus*). *Journal of Experimental Biology* **207**, 869–879.
983
- 984 Marsh, O. C. 1881. Classification of the Dinosauria. *American Journal of Science*
985 (series 3) **23**, 241–244.
986
- 987 Martill, D.M. 1985. Plesiosaur discovery in Scotland. *Geology Today*, 162.
988
- 989 Marshall, P. 2005. Theropod dinosaur and other footprints from the Valtos
990 Sandstone Formation (Bathonian, Middle Jurassic) of the Isle of Skye. *Scottish*
991 *Journal of Geology* **41**, 97–104.
992
- 993 McGowan, C. & Motani, R. 2003. *Ichthyopterygia*. *Handbook of Paleoherpétology*,
994 *Part 8*. Munich, Germany: Verlag Dr. Friedrich Pfeil.
995
- 996 Miller, H. 1858. *The Cruise of the Betsey, or A Summer Ramble Among the*
997 *Fossiliferous Deposits of the Hebrides, and Rambles of a Geologist, or Ten*
998 *Thousand Miles over the Fossiliferous Deposits of Scotland*. Edinburgh, Scotland:
999 NMS Publishing, Edinburgh, 2003 (facsimile of text first published 1858).
1000
- 1001 Mitchell, J. & P. M. Sander. 2014. The three-front model: a developmental
1002 explanation of long bone diaphyseal histology of Sauropoda: Three-Front Model of
1003 Long Bone Histology. *Biological Journal of the Linnean Society* **112**, 765–781.
1004
- 1005 Nacarino-Meneses, C., Jordana, X. & Köhler, M. 2016. Histological variability in the
1006 limb bones of the Asiatic wild ass and its significance for life history inferences.
1007 *PeerJ* 4:e2580.
1008
- 1009 Nopcsa, F. 1915. Die Dinosaurier der siebenbürgische Landesteile Ungarns.
1010 *Mitteilungen aus dem Jahrbüchle der Königlich Ungarischen Geologischen*
1011 *Reichsanstalt* **23**, 1–26.
1012

- 1013 Norman, D. B. 1984. A systematic reappraisal of the reptile order Ornithischia. *In*
1014 Reif, W. -E. & Westphal, F. (eds) *Third Symposium on Mesozoic Terrestrial*
1015 *Ecosystems, Short Papers*, 157–162. Tübingen, Germany: Attempto Verlag.
1016
- 1017 Ósi, A., Prondvai, E., Butler, R. & Weishampel, D. B. 2012. Phylogeny, Histology and
1018 Inferred Body Size Evolution in a New Rhabdodontid Dinosaur from the Late
1019 Cretaceous of Hungary. *PLoS ONE* **7**, e44318
1020
- 1021 Owen, R. 1842. Report on British fossil reptiles. Part II. *Reports of the British*
1022 *Association for the Advancement of Science* **1841**, 60–204.
1023
- 1024 Padian, K. & Lamm, E. -T. 2013. *Bone Histology of Fossil Tetrapods: Advancing*
1025 *Methods, Analysis, and Interpretation*. Berkeley, USA: University of California Press.
1026
- 1027 Padian, K., Horner, J. R. & De Ricqlès, A. 2004. Growth in small dinosaurs and
1028 pterosaurs: the evolution of archosaurian growth strategies. *Journal of Vertebrate*
1029 *Paleontology* **24**, 555–571.
1030
- 1031 Panciroli, E., Benson, R. B. J. & Walsh, S. 2017a. The dentary of *Wareolestes rex*
1032 (Megazostrodonidae): a new specimen from Scotland and implications for
1033 morganucodontan tooth replacement. *Papers in Palaeontology* **3**, 373–386.
1034
- 1035 Panciroli, E., Walsh, S., Fraser, N., Brusatte, S. L. & Corfe, I. 2017b. A
1036 reassessment of the postcanine dentition and systematics of the tritylodontid
1037 *Stereognathus* (Cynodontia, Tritylodontidae, Mammaliaforma), from the Middle
1038 Jurassic of the United Kingdom. *Journal of Vertebrate Paleontology* **37**, e1351448.
1039
- 1040 Panciroli, E., Benson, R. B. J. & Butler, R. J. 2018a. New partial dentaries of
1041 amphitheriid mammal *Palaeoxonodon ooliticus* from Scotland, and posterior dentary
1042 morphology in early cladotherians. *Acta Palaeontologica Polonica* **63**, 197–206.
1043
- 1044 Panciroli, E., Benson, R. B. J. & Walsh, S. 2018b. The mammal-rich freshwater
1045 assemblage of the Middle Jurassic Kilmaluag Formation, Isle of Skye, Scotland. *13th*
1046 *Symposium on Mesozoic Terrestrial Ecosystems and Biota, Abstracts*. Bonn,
1047 Germany.
1048
- 1049 Panciroli, E., Benson, R. B. J. & Luo, Z. -X. 2019. The mandible and dentition of
1050 *Boreolestes serendipitus* (Docodonta) from the Middle Jurassic of Skye, Scotland.
1051 *Journal of Vertebrate Paleontology* **39**, e1621884.
1052
- 1053 Raven, T. J. & Maidment, S. C. R. 2017. A new phylogeny of Stegosauria
1054 (Dinosauria: Ornithischia). *Palaeontology* **60**, 401–408.
1055

- 1056 Redelstorff, R. & Sander, P. M. 2009. Long and girdle bone histology of
1057 *Stegosaurus*: implications for growth and life history. *Journal of Vertebrate*
1058 *Paleontology* **29**, 1087–1099.
- 1059
- 1060 Redelstorff, R., Hübner, T. R., Chinsamy, A. & Sander, P. M. 2013. Bone Histology
1061 of the Stegosaur *Kentrosaurus aethiopicus* (Ornithischia: Thyreophora) from the
1062 Upper Jurassic of Tanzania. *The Anatomical Record* **296**, 933–952.
- 1063
- 1064 Rees J. & Underwood, C. J. 2005. Hybodont sharks from the Middle Jurassic of the
1065 Inner Hebrides, Scotland. *Earth and Environmental Science Transactions of the*
1066 *Royal Society of Edinburgh* **96**, 351–363.
- 1067
- 1068 Remes, K., Ortega, F., Fierro, I., Joger, U., Kosma, R., Ferrer, J. M. M., Ide, O. A. &
1069 Maga, A., 2009. A new basal sauropod dinosaur from the Middle Jurassic of Niger
1070 and the early evolution of Sauropoda. *PLoS One* **4**, e6924.
- 1071
- 1072 de Ricqlès, A. J. 1983. Cyclical growth in the long limb bones of a sauropod
1073 dinosaur. *Acta Palaeontologica Polonica* **28**, 225–232.
- 1074
- 1075 de Ricqlès, A., Padian, K., Horner, J. R. & Francillon-Vieillot, H. 2000.
1076 Palaeohistology of the bones of pterosaurs (Reptilia: Archosauria): anatomy,
1077 ontogeny, and biomechanical implications. *Zoological Journal of the Linnean Society*
1078 **129**, 349–385.
- 1079
- 1080 de Ricqlès, A. J., Padian, K. & Horner, J. R. 2003. On the bone histology of some
1081 Triassic pseudosuchian archosaurs and related taxa. *Annales de Paléontologie* **89**,
1082 67–101.
- 1083
- 1084 Riding, J. B., Walton, W. & Shaw, D. 1991. Toarcian to Bathonian (Jurassic
1085 Palynology of the Inner Herides, Northwest Scotland. *Palynology* **15**, 115–179.
- 1086
- 1087 Sadlier, R., Barrett, P. M. & Powell, H. P. 2008. The anatomy and systematics of
1088 *Eustreptospondylus oxoniensis*, a theropod dinosaur from the Middle Jurassic of
1089 Oxfordshire, England. *Monograph of the Palaeontographical Society* **160**, 1–82.
- 1090 Sander, P. M. 2000. Longbone histology of the Tendaguru sauropods: implications
1091 for growth and biology. *Paleobiology* **26**, 466–488.
- 1092
- 1093 Sander, P. 2004. Adaptive radiation in sauropod dinosaurs: bone histology indicates
1094 rapid evolution of giant body size through acceleration. *Organisms Diversity &*
1095 *Evolution* **4**, 165–173.
- 1096
- 1097 Sander, P. M., Mateus, O., Laven, T. & Knötschke, N. 2006. Bone histology indicates
1098 insular dwarfism in a new Late Jurassic sauropod dinosaur. *Nature* **441**, 739–741.
- 1099

- 1100 Sander, P. M., Klein, N., Stein, K. W. H. & Wings O. 2011. Sauropod bone histology
1101 and its implications for sauropod biology. *In* Klein, N., Remes, K., Gee, C. & Sander,
1102 P. M. (eds) *Biology of the Sauropod Dinosaurs: Understanding the Life of Giants*,
1103 276–304. Bloomington, USA: Indiana University Press.
- 1104
- 1105 Sander, P. M., Christian, A., Clauss, M., Fechner, R., Gee, C. T., Griebeler, E. M.,
1106 Gunga, H. C., Hummel, J., Mallison, H., Perry, S. F. & Preuschoft, H. 2011. Biology
1107 of the sauropod dinosaurs: the evolution of gigantism. *Biological Reviews* **86**, 117–
1108 155.
- 1109
- 1110 Sayão, J. M., Bantim, R. A. M., Andrade, R. C. L. P., Lima, F. J., Saraiva, A. A. F.,
1111 Figueiredo, R. G. & Kellner, A. W. A. 2016. Paleohistology of *Susisuchus anatoceps*
1112 (Crocodylomorpha, Neosuchia): Comments on Growth Strategies and Lifestyle.
1113 *PLOS ONE* **11**, e0155297.
- 1114
- 1115 Seeley, H. G. 1887. On the classification of the fossil animals commonly named
1116 Dinosauria. *Proceedings of the Royal Society of London* **43**, 165–171.
- 1117
- 1118 Stein, K., Csiki, Z., Rogers, K. C., Weishampel, D. B., Redelstorff, R., Carballido, J.
1119 L. & Sander, P. M. 2010. Small body size and extreme cortical bone remodeling
1120 indicate phyletic dwarfism in *Magyarosaurus dacus* (Sauropoda: Titanosauria).
1121 *Proceedings of the National Academy of Sciences* **107**, 9258–9263.
- 1122
- 1123 Stein, K. W. H. & Werner, J. 2013. Preliminary Analysis of Osteocyte Lacunar
1124 Density in Long Bones of Tetrapods: All Measures Are Bigger in Sauropod
1125 Dinosaurs. *PLoS ONE* **8**, e77109.
- 1126
- 1127 Stein, M., Hayashi, S. & Sander, P. M. 2013. Long Bone Histology and Growth
1128 Patterns in Ankylosaurs: Implications for Life History and Evolution. *PLoS ONE* **8**,
1129 e68590.
- 1130
- 1131 Upchurch, P. & Martin, J. 2002. The Rutland *Cetiosaurus*: the anatomy and
1132 relationships of a Middle Jurassic British sauropod dinosaur. *Palaeontology* **45**,
1133 1049–1074.
- 1134
- 1135 Upchurch, P. & Martin, J. 2003. The anatomy and taxonomy of *Cetiosaurus*
1136 (Saurischia, Sauropoda) from the Middle Jurassic of England. *Journal of Vertebrate*
1137 *Paleontology* **23**, 208–231.
- 1138
- 1139 Upchurch, P., Barrett, P. M. & Dodson, P. 2004. Sauropoda. *In* Weishampel, D.B.,
1140 Dodson, P. & Osmólska, H. (eds) *The Dinosauria. Second Edition*, 259–322.
1141 Berkeley, USA: University of California Press.
- 1142

- 1143 Uytterschaut, H. 1993. Human Bone Remodelling and Aging. *In* Grupe, G. &
1144 Garland, A. N. (eds) *Histology of Ancient Human Bone: Methods and Diagnosis*, 95–
1145 109. Berlin, Germany: Springer.
1146
- 1147 Weishampel, D. B., Barrett, P. M., Coria, R. A., Le Loeuff, J., Xing, X., Xijin, Z.,
1148 Sahni, A., Gomani, E. M. & Noto, C.R. 2004. Dinosaur distribution. *In* Weishampel,
1149 D.B., Dodson, P. & Osmolska, H. (eds) *The Dinosauria*. 2nd edn, 517–606. Berkeley,
1150 USA: University of California Press.
1151
- 1152 Werning, S. 2012. The Ontogenetic Osteohistology of *Tenontosaurus tilletti*. *PLoS*
1153 *ONE* **7**, e33539.
1154
- 1155 Wilberg, E. W. 2015. A new metriorhynchoid (Crocodylomorpha, Thalattosuchia)
1156 from the Middle Jurassic of Oregon and the evolutionary timing of marine
1157 adaptations in thalattosuchian crocodylomorphs. *Journal of Vertebrate Paleontology*
1158 **35**, e902846.
1159
- 1160 Wilkinson, M. 1992. Concretionary cements in Jurassic sandstones, Isle of Eigg,
1161 Inner Hebrides. *Geological Society, London, Special Publications* **62**, 145–154.
1162
- 1163 Wills, S., Barrett, P. M. & Walker, A. 2014. New dinosaur and crocodylomorph from
1164 the Middle Jurassic (Bathonian) Kilmaluag Formation, Skye, Scotland. *Scottish*
1165 *Journal of Geology* **50**, 183–190.
1166
- 1167 Wintrich, T., Hayashi, S. Houssaye, A., Nakajima, Y. & Sander, P. M. 2017. A
1168 Triassic plesiosaurian skeleton and bone histology inform on evolution of a unique
1169 body plan. *Science Advances* **3**, e1701144.
1170
- 1171 Woodward, H. N. 2019. *Maiasaura* (Dinosauria: Hadrosauridae) tibia osteohistology
1172 reveals non-annual cortical vascular rings in young of the year. *Frontiers in Earth*
1173 *Science* **7**, 50.
1174
- 1175 Woodward, H. N. & Lehman, T. M. 2009. Bone histology and microanatomy of
1176 *Alamosaurus sanjuanensis* (Sauropoda: Titanosauria) from the maastrichtian of Big
1177 Bend National Park, Texas. *Journal of Vertebrate Paleontology* **29**, 807–821.
1178
- 1179 Woodward, H. N., Horner, J. R. and Farlow, J. O. 2011. Osteohistological evidence
1180 for determinate growth in the American alligator. *Journal of Herpetology* **45**, 339–
1181 342.
1182
- 1183 Woodward, H. N., Horner, J. R. & Farlow, J. O. 2014. Quantification of intraskeletal
1184 histovariability in *Alligator mississippiensis* and implications for vertebrate
1185 osteohistology. *PeerJ* **2**, e422.
1186

- 1187 Woodward, H. N., Rich, T. H. & Vickers-Rich P. 2018. The bone microstructure of
 1188 polar “hypsilophodontid” dinosaurs from Victoria, Australia. *Scientific Reports* **8**, 1–
 1189 14.
 1190
- 1191 Woodward, H. N., Freedman Fowler, E. A., Farlow, J. O., & Horner, J. R. 2015.
 1192 *Maiasaura*, a model organism for extinct vertebrate population biology: a large
 1193 sample statistical assessment of growth dynamics and survivorship. *Paleobiology*
 1194 **41**, 503–527.
 1195
- 1196 Yi, H., Tennant, J. P., Young, M. T., Challands, T. J., Foffa, D., Hudson, J. D., Ross,
 1197 D. A. & Brusatte, S. L., 2017. An unusual small-bodied crocodyliform from the Middle
 1198 Jurassic of Scotland, UK, and potential evidence for an early diversification of
 1199 advanced neosuchians. *Earth and Environmental Science Transactions of the Royal*
 1200 *Society of Edinburgh* **107**, 1–12.
 1201
- 1202 Young, M.T., Tennant, J.P., Brusatte, S.L., Challands, T.J., Fraser, N.C., Clark, N.D.
 1203 & Ross, D.A., 2016a. The first definitive Middle Jurassic atoposaurid
 1204 (Crocodylomorpha, Neosuchia), and a discussion on the genus *Theriosuchus*.
 1205 *Zoological journal of the Linnean Society* **176**, 443–462.
 1206
- 1207 Young, M. T., Márton, R., Bell, M. A., Foffa, D., Steel, L., Sachs, S. & Peyer, K.
 1208 2016b. Big-headed marine crocodyliforms and why we must be cautious when using
 1209 extant species as body length proxies for long-extinct relatives. *Palaeontologia*
 1210 *Electronica* **19**, 1–14.
 1211
- 1212 Young, C. M. E., Hendrickx, C., Challands, T. J., Foffa, D., Ross, D. A., Butler, I. B.
 1213 & Brusatte, S. L. 2019. New theropod dinosaur teeth from the Middle Jurassic of the
 1214 Isle of Skye, Scotland. *Scottish Journal of Geology* **55**, 7–19.
 1215

1217 Figure captions

1218

1219 **Figure 1.** The lithostratigraphy of the Great Estuarine Group and location **at Camas**
 1220 **Sgjetaig on the Isle of Eigg where** NMS.Eigg.2017 was found.
 1221

1222 **Figure 2.** NMS.Eigg.2017, **a probable** thyreophoran limb bone from the Isle of Eigg,
 1223 Scotland. A, NMS.Eigg.2017 in matrix after initial prep. B-E, NMS.Eigg.2017
 1224 removed from matrix and partially reconstructed: B, the eroded ‘upper’ surface; C,
 1225 the surface that was downwards into the matrix; D and E, side views of
 1226 NMS.Eigg.2017. Scale bar B-E same = 100 mm.
 1227

1228 **Figure 3.** Possible bite marks (indicated by arrows) **A**, and molluscs **B** on underside
 1229 of NMS.Eigg.2017
 1230

1231 **Figure 4.** Postcranial elements of theropod dinosaurs *Megalosaurus* and
 1232 *Eustreptospondylus*. *Megalosaurus bucklandii* NHMUK PV OR31806 femur 31806
 1233 anterior **A**, and posterior **B**, view; *Eustreptospondylus oxoniensis* OUMNH J.13558
 1234 femur in anterior **C**, and posterior **D** view; *Megalosaurus bucklandii* OUMNH J.13575
 1235 humerus in anterior view **E**; and *Megalosaurus bucklandii* NHMUK PV OR31809 tibia
 1236 in anterior **F**, and posterior **G** view. All scale bars 100 mm.

1237
 1238 **Figure 5.** Postcranial elements of sauropod dinosaurs. *Cetiosaurus oxoniensis*
 1239 femur OUMNH J.13615 in posterior view **A**; *Barapasaurus tagorei* ISIR741 femur in
 1240 anterior view **B** and posterior view **C**; *Cetiosaurus oxoniensis* OUMNH J.29807 fibula
 1241 in anterior view **D**; *Rhoetosaurus brownei* QMF 1659 fibula in anterior **E** and
 1242 posterior **F** view; *Spinophrosaurus nigerensis* GCP-CV-4429 fibula in anterior view
 1243 **G**; *Tazoudasaurus naimi* pT-1 humerus in anterior view in anterior **H** and posterior **I**
 1244 view; *Cetiosaurus oxoniensis* OUMNH J.13611 ulna **J** and radius **K** in anterolateral
 1245 view. Scale bar same throughout = 100 mm.

1246
 1247 **Figure 6.** Postcranial elements of thyreophoran dinosaurs. Anterior views of
 1248 *Stegosaurus stenops* NHMUK PV R36730 femora **A**, humerus **C**, ulna **E**, radius **G**,
 1249 fused tibia and fibula **I**; anterior view of *Edmontonia* sp. CMN 8531 femur **B**; anterior
 1250 view of *Euoplocephalus tutus* AMNH 5337 humerus **D** and radius **H**; anterior view of
 1251 *Euoplocephalus tutus* AMNH 5403 ulna **F**; anterior view of *Polacanthus foxii* NHMUK
 1252 PV R175 tibia with partial fibula fused to distal end **J**; posterior view of *Ankylosaurus*
 1253 *magniventris* AMNH 5214 fibula **K**. Scale bar equal to 100 mm.

1254
 1255 **Figure 7.** Overview of the osteohistology of NMS.Eigg.2017. **A**, column through the
 1256 cortex, showing medullary spaces endosteally, dense Haversian bone throughout
 1257 most of the cortex, and primary fibrolamellar bone in the outer cortex; **B**, overview of
 1258 entire slide, showing the arrangement of the medullary cavity and the cortex, and
 1259 position of the LAG (arrow) in the middle cortex; **C**, outer cortex, showing primary
 1260 fibrolamellar bone with longitudinal–reticular vascularity and consistent vascularity to
 1261 the periosteal surface; **D**, outer cortex, showing zone of dense Haversian bone
 1262 grading into primary fibrolamellar bone with a LAG (arrow), and a second, isolated
 1263 zone of secondary remodelling. All images under normal light. Abbreviations: FLB,
 1264 fibrolamellar bone; HB, Haversian bone; LAG, line of arrested growth; longvasc,
 1265 longitudinal vascularity; Retvasc, reticular vascularity; SOs, secondary osteons; SR,
 1266 secondary remodelling.

1267
 1268 **Figure 8.** Histological details of NMS.Eigg.2017. **A**, primary osteons in the outer
 1269 cortex, showing fibrolamellar bone matrix and variation in osteocyte shape and
 1270 density; **B**, primary and secondary osteons with a LAG (arrow) in the outer cortex; **C**,
 1271 overlapping generations of secondary osteons within the dense Haversian bone of
 1272 the inner cortex; numbers indicate order of deposition; **D**, trabeculae composed of
 1273 lamellar bone and infilled with endosteal lamellae in the medullary cavity; **E**, **erosive**
 1274 **cavities in the fibrolamellar bone separating the two zones of secondary remodelling;**

1275 **F**, outer cortex, showing consistent vascular orientation and density, localized
 1276 secondary remodelling, and erosional cavities. All images under normal light.
 1277 Abbreviations: **ec**, erosional cavity; el, endosteal lamellae; lb, lamellar bone; po,
 1278 primary osteon; so, secondary osteon; **sr**, secondary remodelling; **vasc**, vascular
 1279 canal; **wb**, woven bone.

1280

1281

1282 **Tables**

1283

1284 **Table 1.** Measurements of NMS.Eigg.2017 and other Middle Jurassic dinosaur limb
 1285 bones. Data from Benson (2010), Holwerda *et al.* (in press) Remes *et al.* (2009) and
 1286 author's own photographs of specimens. *Measurements are estimated due to
 1287 missing proximal and distal ends of NMS.Eigg.2017 and compression and erosion of
 1288 mid-shaft, and should be considered with caution.

1289

Taxon	Specimen	Bone	Length (cm)	Width (mid shaft) (cm)	L/W ratio
Eigg Dinosaur	NMS.Eigg.2017	-	64-79*	7.3*	0.11-0.09
<i>Megalosaurus bucklandii</i>	OUMNH J.13575	humerus	39	6	0.15
<i>Megalosaurus bucklandii</i>	NHMUK PV OR36585	ulna	23	5	0.22
<i>Megalosaurus bucklandii</i>	NHMUK PV OR31806	femur	81	10	0.12
<i>Megalosaurus bucklandii</i>	NHMUK PV OR31809	tibia	65	7	0.11
<i>Cetiosaurus oxoniensis</i>	OUMNH J.13612	ulna	121	19	0.16
<i>Cetiosaurus oxoniensis</i>	OUMNH J.13615	femur	166	30	0.18
<i>Cetiosaurus oxoniensis</i>	OUMNH J.29807	fibula	57	6	0.11
<i>Cetiosaurus oxoniensis</i>	OUMNH J.13621	tibia	96	17	0.18
<i>Barapasaurus tagorei</i>	ISIR 70	humerus	84	12	0.14
<i>Barapasaurus tagorei</i>	ISIR 72	ulna	60	7	0.12
<i>Barapasaurus tagorei</i>	ISIR 71	radius	55	6	0.11
<i>Barapasaurus tagorei</i>	ISIR 64	fibula	55	4	0.07
<i>Barapasaurus tagorei</i>	ISIR 741	femur	93	13	0.14
<i>Spinophorosaurus nigerensis</i>	NMB-1698-R	humerus	60	8	0.13
<i>Spinophorosaurus nigerensis</i>	GCP-CV-4229/NMB-1699-R	femur	64	10	0.16
<i>Spinophorosaurus nigerensis</i>	GCP-CV-4229/NMB-1699-R	fibula	36	4	0.11

1290

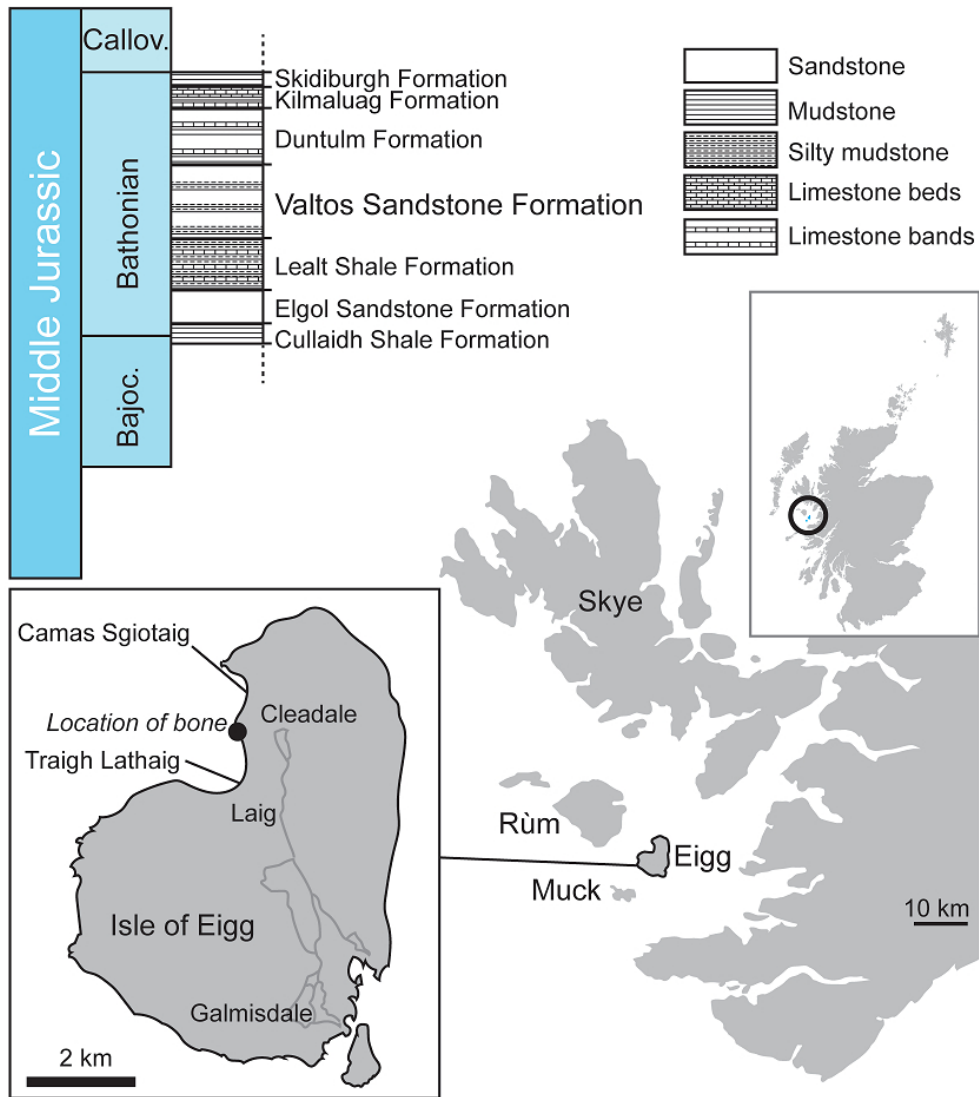


Figure 1. The lithostratigraphy of the Great Estuarine Group and location NMS.Eigg.2017 was found.

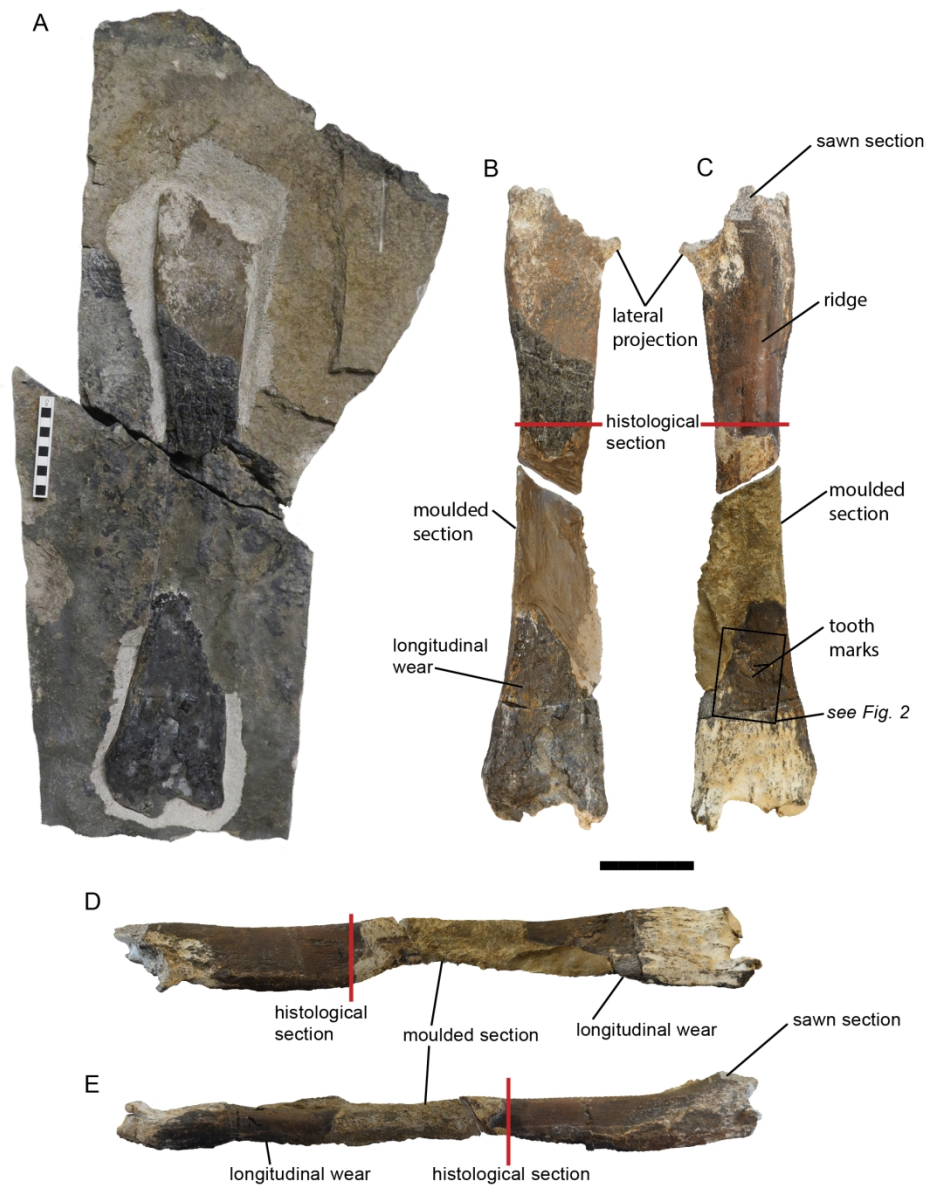


Figure 2. NMS.Eigg.2017, a probable thyreophoran limb bone from the Isle of Eigg, Scotland. A, NMS.Eigg.2017 in matrix after initial prep. B-E, NMS.Eigg.2017 removed from matrix and partially reconstructed: B, the eroded 'upper' surface; C, the surface that was downwards into the matrix; D and E, side views of NMS.Eigg.2017. Scale bar B-E same = 100 mm.

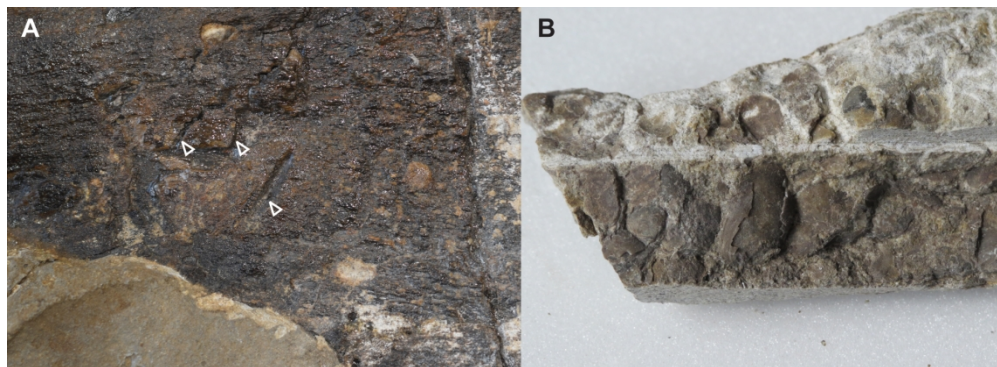


Figure 3. Bite marks (indicated by arrows) A, and molluscs B on underside of NMS.Eigg.2017.

685x249mm (72 x 72 DPI)



Figure 4. Postcranial elements of theropod dinosaurs *Megalosaurus* and *Eustreptospondylus*. *Megalosaurus bucklandii* NHMUK PV OR31806 femur 31806 anterior A, and posterior B, view; *Eustreptospondylus oxoniensis* OUMNH J.13558 femur in anterior C, and posterior D view; *Megalosaurus bucklandii* OUMNH J.13575 humerus in anterior view E; and *Megalosaurus bucklandii* NHMUK PV OR31809 tibia in anterior F, and posterior G view. All scale bars 100 mm.

693x932mm (72 x 72 DPI)



Figure 5. Postcranial elements of sauropod dinosaurs. *Cetiosaurus oxoniensis* femur OUMNH J.13615 in posterior view A; *Barapasaurus tagorei* ISIR741 femur in anterior view B and posterior view C; *Cetiosaurus oxoniensis* OUMNH J.29807 fibula in anterior view D; *Rhoetosaurus brownei* QMF 1659 fibula in anterior E and posterior F view; *Spinophrosaurus nigerensis* GCP-CV-4429 fibula in anterior view G; *Tazoudasaurus naimi* pT-1 humerus in anterior view in anterior H and posterior I view; *Cetiosaurus oxoniensis* OUMNH J.13611 ulna J and radius K in anterolateral view. Scale bar same throughout = 100 mm.

667x1051mm (72 x 72 DPI)

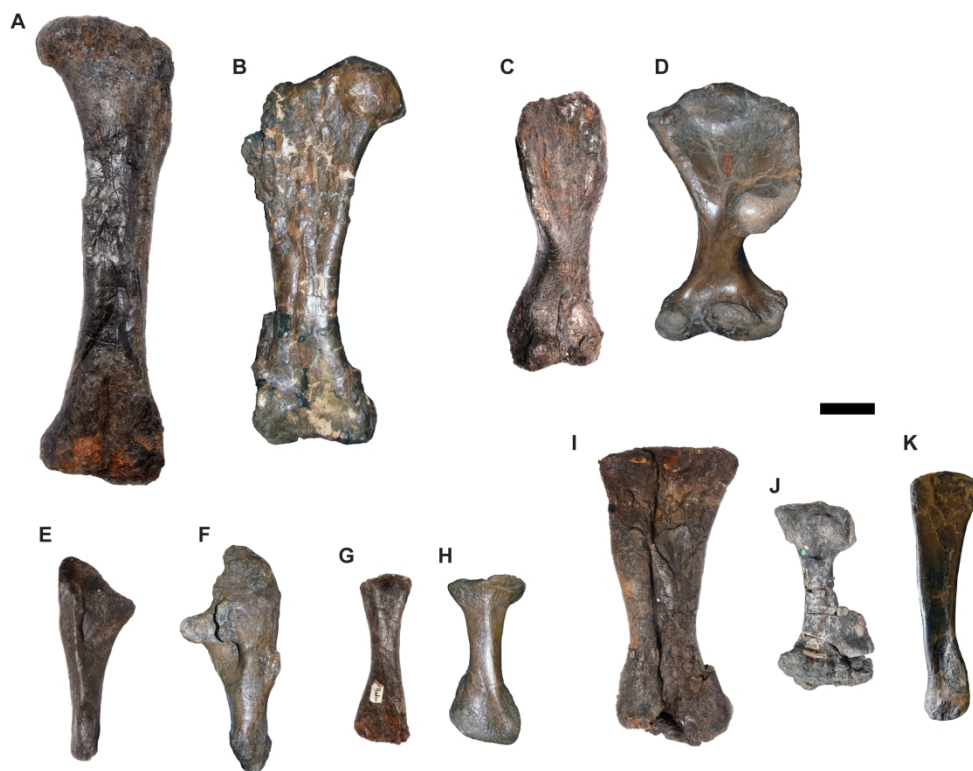


Figure 6. Postcranial elements of thyreophoran dinosaurs. Anterior views of *Stegosaurus stenops* NHMUK PV R36730 femora A, humerus C, ulna E, radius G, fused tibia and fibula I; anterior view of *Edmontonia* sp. CMN 8531 femur B; anterior view of *Euoplocephalus tutus* AMNH 5337 humerus D and radius H; anterior view of *Euoplocephalus tutus* AMNH 5403 ulna F; anterior view of *Polacanthus foxii* NHMUK PV R175 tibia with partial fibula fused to distal end J; posterior view of *Ankylosaurus magniventris* AMNH 5214 fibula K. Scale bar equal to 100 mm.

841x657mm (72 x 72 DPI)

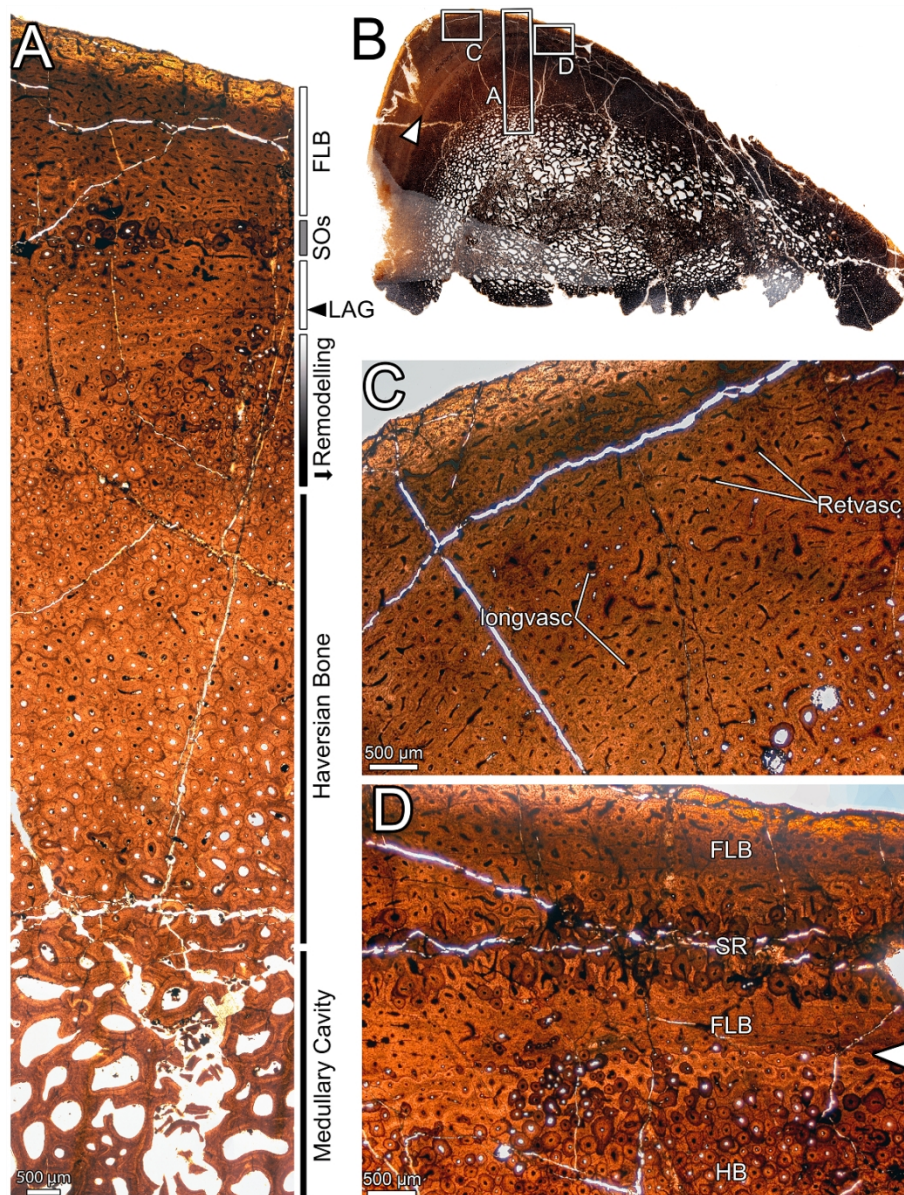


Figure 7. Overview of the osteohistology of NMS.Eigg.2017. A, column through the cortex, showing medullary spaces endosteally, dense Haversian bone throughout most of the cortex, and primary fibrolamellar bone in the outer cortex; B, overview of entire slide, showing the arrangement of the medullary cavity and the cortex, and position of the LAG (arrow) in the middle cortex; C, outer cortex, showing primary fibrolamellar bone with longitudinal–reticular vascularity and consistent vascularity to the periosteal surface; D, outer cortex, showing zone of dense Haversian bone grading into primary fibrolamellar bone with a LAG (arrow), and a second, isolated zone of secondary remodelling. All images under normal light. Abbreviations: FLB, fibrolamellar bone; HB, Haversian bone; LAG, line of arrested growth; longvasc, longitudinal vascularity; Retvasc, reticular vascularity; SOs, secondary osteons; SR, secondary remodelling.

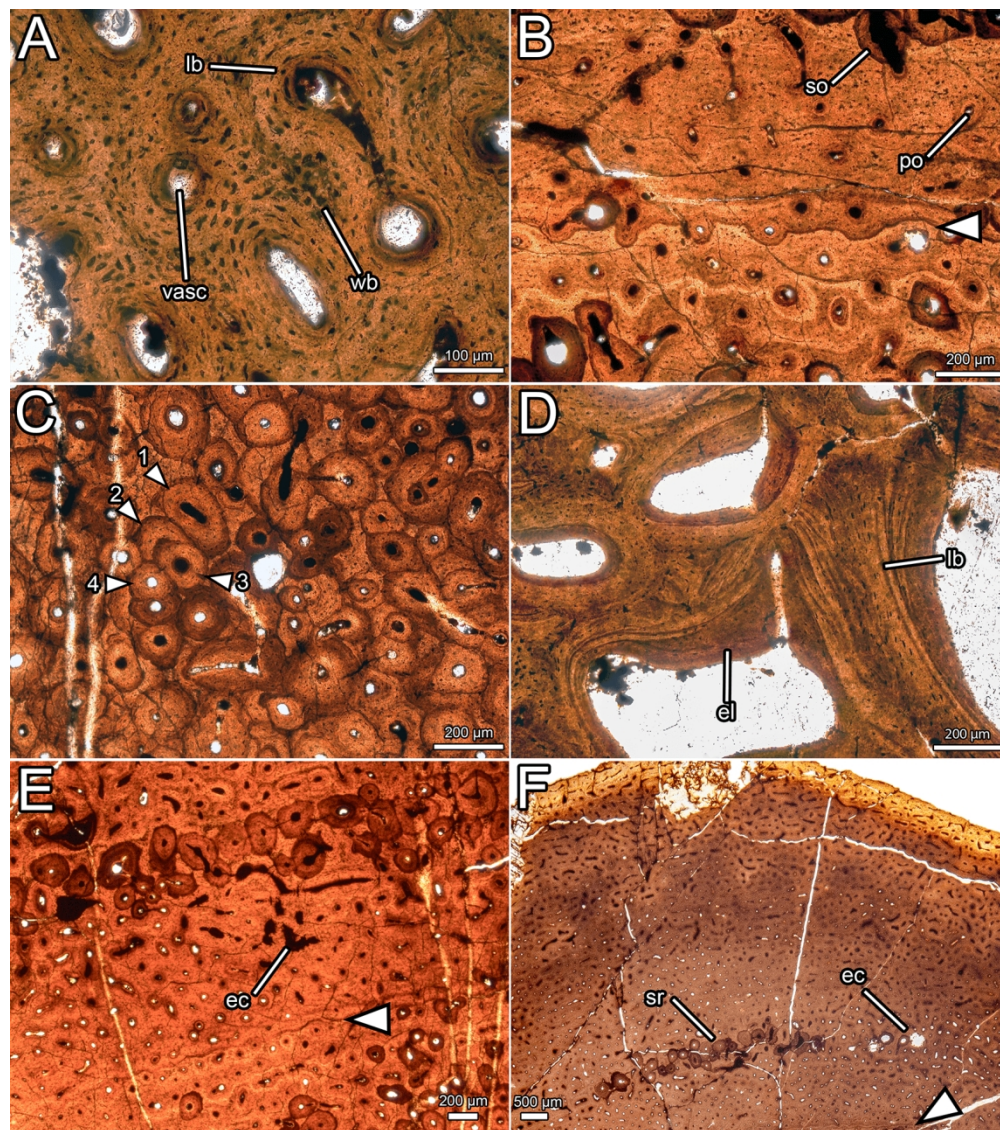


Figure 8. Histological details of NMS.Eigg.2017. A, primary osteons in the outer cortex, showing fibrolamellar bone matrix and variation in osteocyte shape and density; B, primary and secondary osteons with a LAG (arrow) in the outer cortex; C, overlapping generations of secondary osteons within the dense Haversian bone of the inner cortex; numbers indicate order of deposition; D, trabeculae composed of lamellar bone and infilled with endosteal lamellae in the medullary cavity; E, erosive cavities in the fibrolamellar bone separating the two zones of secondary remodelling; F, outer cortex, showing consistent vascular orientation and density, localized secondary remodelling, and erosional cavities. All images under normal light. Abbreviations: ec, erosional cavity; el, endosteal lamellae; lb, lamellar bone; po, primary osteon; so, secondary osteon; sr, secondary remodelling; vasc, vascular canal; wb, woven bone.

608x685mm (72 x 72 DPI)